THE JOURNAL OF BIOLOGICAL CHEMISTRY VOL. 286, NO. 13, pp. 11616–11631, April 1, 2011

Hair Follicular Expression and Function of Group X Secreted Phospholipase A_2 in Mouse Skin*[S]

Received for publication, November 25, 2010, and in revised form, January 17, 2011 Published, JBC Papers in Press, January 25, 2011, DOI 10.1074/jbc.M110.206714

Kei Yamamoto,[a] Yoshitaka Taketomi,[a,b] Yuki Isogai,[a,c] Yoshimi Miki,[a,b] Hiroyasu Sato,[a,b] Seiko Masuda,[a,b] Yasumasa Nishito,[d] Kiyokazu Morioka,[e1] Yoshikazu Ishimoto,[f] Noriko Suzuki,[f] Yasunori Yokota,[f] Kohji Hanasaki,[f] Yukio Ishikawa,[g] Toshiharu Ishii,[g] Tetsuyuki Kobayashi,[c] Kiyoko Fukami,[h] Kazutaka Ikeda,[i,j] Hiroki Nakanishi,[i,j] Ryo Taguchi,[i,j] and Makoto Murakami[a,k2]

From the [a]Lipid Metabolism Project, [d]Core Technology and Research Center and the [e]Electron Microscope Laboratory, the Tokyo Metropolitan Institute of Medical Science, 2-1-6 Kamikitazawa, Setagaya-ku, Tokyo 156-8506, the [b]Department of Health Chemistry, School of Pharmaceutical Sciences, Showa University, 1-5-8 Hatanodai, Shinagawa-ku, Tokyo 142-8555, the [c]Department of Biology, Faculty of Science, Ochanomizu University, 2-1-1 Otsuka, Bunkyo-ku, Tokyo 112-8610, [f]Shionogi Research Laboratories, Shionogi and Company Ltd, 3-1-1, Futaba-cho, Toyonaka, Osaka 561-0825, the [g]Department of Pathology, Toho University School of Medicine, 5-21-16 Omori-Nishi, Ohta-ku, Tokyo 143-8540, the [h]Laboratory of Genome and Biosignal, Tokyo University of Pharmacy and Life Science, 1432-1 Horinouchi, Hachioji, 192-0392 Tokyo, the [i]Department of Metabolome, Graduate School of Medicine, The University of Tokyo, 7-3-1 Hongo, Bunkyo-ku, Tokyo 113-0033, and [j]CREST and [k]PRESTO, Japan Science and Technology Agency, 4-1-8 Honcho, Kawaguchi, Saitama 332-0012, Japan

Although perturbed lipid metabolism can often lead to skin abnormality, the role of phospholipase A_2 (PLA_2) in skin homeostasis is poorly understood. In the present study we found that group X-secreted PLA_2 ($sPLA_2$-X) was expressed in the outermost epithelium of hair follicles in synchrony with the anagen phase of hair cycling. Transgenic mice overexpressing $sPLA_2$-X (*PLA2G10*-Tg) displayed alopecia, which was accompanied by hair follicle distortion with reduced expression of genes related to hair development, during a postnatal hair cycle. Additionally, the epidermis and sebaceous glands of *PLA2G10*-Tg skin were hyperplasic. Proteolytic activation of $sPLA_2$-X in *PLA2G10*-Tg skin was accompanied by preferential hydrolysis of phosphatidylethanolamine species with polyunsaturated fatty acids as well as elevated production of some if not all eicosanoids. Importantly, the skin of *Pla2g10*-deficient mice had abnormal hair follicles with noticeable reduction in a subset of hair genes, a hypoplasic outer root sheath, a reduced number of melanin granules, and unexpected up-regulation of prostanoid synthesis. Collectively, our study highlights the spatiotemporal expression of $sPLA_2$-X in hair follicles, the presence of skin-specific machinery leading to $sPLA_2$-X activation, a functional link of $sPLA_2$-X with hair follicle homeostasis, and compartmentalization of the prostanoid pathway in hair follicles and epidermis.

Hair follicle morphogenesis is regulated by interactions between epidermal keratinocytes committed to hair follicle differentiation and dermal fibroblasts committed to form the dermal papilla of the developing hair follicles (1–3). These epithelial-mesenchymal interactions culminate in the formation of the hair shaft, which is surrounded by the multilayered inner root sheath (IRS)[3] and outer root sheath (ORS), the latter being the outermost concentric layer of epithelial cells. Hair follicles undergo repeated cycles of growth (anagen), regression (catagen), and rest (telogen) during their life span. Distinct signaling pathways and transcription factors control hair follicle morphogenesis, postnatal hair growth, and hair cycling in a coordinated manner. Accordingly, disturbance in the expression or function of these genes by point mutations, transgenic (Tg) overexpression, or targeted disruption often culminates in a hairless phenotype. Because hair loss due to various factors, such as diseases, hormonal imbalance, and drug regimens, affects a large population worldwide, there are compelling reasons to understand the fundamentals of hair biology.

Current evidence suggests that, in addition to a variety of cytokines and growth factors (4, 5), lipids also play important roles in hair follicle homeostasis (6, 7). The PGE_2 receptors EP3 and EP4 are expressed in the dermal papilla and ORS of hair follicles (8, 9). COX-2 displays a trend of hair cycle-synchronized expression in the ORS of hair follicles (9), and skin-specific Tg overexpression of COX-2 leads to delayed emergence of hair shafts, reduced hair follicle density, and alopecia (10, 11). Elevated expression of EP4 and COX-2 has been found in biopsy samples from patients with scarring alopecia (12). These observations suggest that excess PGE_2 signaling is detrimental for hair homeostasis. Autosomal recessive wooly hair with

* This work was supported by grants-in aid for Scientific Research (to M. M.) and for Young Investigators (to K. Y., Y. T., and H. S.) from the Ministry of Education, Science, Culture, Sports, and Technology of Japan, SHISEIDO Grants for Scientific Research (to K. Y.), PRESTO (to M. M.), and CREST (to R. T.) from the Japan Science and Technology Agency, and the Cosmetology Research, Nakatomi, Uehara Toray and Mitsubishi Science Foundations (to M. M.).

[S] The on-line version of this article (available at http://www.jbc.org) contains supplemental Tables S1 and S2 and Figs. S1–S6.

[1] Present address: Dept. of Biological Sciences, Tokyo Institute of Technology, 2-12-1 Ookayama, Meguro-Ku, Tokyo 152-8551, Japan.

[2] To whom correspondence should be addressed: Lipid Metabolism Project, The Tokyo Metropolitan Institute of Medical Science, 2-1-6 Kamikitazawa, Setagaya-ku, Tokyo 156-8506, Japan. Tel.: 81-3-5316-3228; Fax: 81-3-5316-3125; E-mail: murakami-mk@igakuken.or.jp.

[3] The abbreviations used are: IRS, inner root sheath; ORS, outer root sheath; Tg, transgenic; PG, prostaglandin; LPA, lysophosphatidic acid; PLA_2, phospholipase A_2; $sPLA_2$, secreted PLA_2; $sPLA_2$-IIA, group IIA $sPLA_2$; $sPLA_2$-X, group X $sPLA_2$; PE, phosphatidylethanolamine; ESI, electrospray ionization; AA, arachidonic acid; PC, phosphatidylcholine; PUFA, polyunsaturated fatty acid; LOX, lipoxygenase; mPGES, microsomal PGE synthase; PPAR, peroxisome proliferator-activating receptor.

hypotrichosis, a type of nonsyndromic human alopecia, is caused by mutations of either *LIPH*, which encodes a phospholipase A_1 that produces lysophosphatidic acid (LPA) from phosphatidic acid, or *P2Y5*, which encodes the LPA_6 receptor (7), implying the importance of LPA signaling in hair growth. In addition, hair abnormalities have often been associated with mutations or altered expression of genes for lipid synthesis, degradation, signaling, or transport (13–16), further highlighting the close connection between lipid perturbation and hair disorders.

Because phospholipase A_2 (PLA_2) regulates the first step of enzymatic cascades, leading to biosynthesis of lipid mediators, and also plays an important role in membrane homeostasis, it is tempting to speculate that certain PLA_2 enzymes would participate in the regulation of hair development. PLA_2s have been classified into several groups, including secreted PLA_2s (sPLA$_2$s), Ca^{2+}-dependent cytosolic PLA_2s, Ca^{2+}-independent PLA_2s, platelet-activating factor acetylhydrolases, and lysosomal PLA_2s (17). Although recent studies employing mice with gene targeting of intracellular and extracellular PLA_2s have delineated their non-redundant functions in various biological events (17, 18), none of these knock-out mice have developed skin abnormalities. The notion that sPLA$_2$ may play a role in skin biology originally arose from studies employing Tg mice overexpressing group IIA sPLA$_2$ (sPLA$_2$-IIA), which develop permanent alopecia and epidermal hyperplasia (19). However, the fact that the mouse strain used so far (C57BL/6) intrinsically lacks sPLA$_2$-IIA because of a frameshift mutation in its gene (20) has raised a question as to the physiological relevance of the hairless phenotype in *PLA2G2A*-Tg mice. Although mammalian genomes encode genes for 10 catalytically active sPLA$_2$ isoforms that exhibit unique tissue and cellular localizations and enzymatic properties (17, 18), it remains uncertain whether other sPLA$_2$ isoforms are expressed and play roles within a skin niche.

Group X sPLA$_2$ (sPLA$_2$-X) is the most active sPLA$_2$ isoform that can hydrolyze phospholipids in the mammalian cell membrane (21). sPLA$_2$-X is synthesized as an enzymatically inactive zymogen, and proteolytic cleavage of the N-terminal propeptide leads to its conversion into the active form (22). Recent studies using *Pla2g10*-deficient mice have revealed its roles in T_{H2}-biased asthma (23), ischemia/perfusion-induced myocardial injury (24), sperm fertility (25), adrenal corticosterone secretion (26), adiposity (27), and aortic aneurysm (28). In the present study, we found that Tg overexpression of sPLA$_2$-X in mice resulted in skin abnormalities characterized by alopecia, unusual hair cycling, and epidermal and sebaceous gland hyperplasia, accompanied by aberrant hydrolysis of phosphatidylethanolamine (PE) and increased synthesis of some eicosanoids. More importantly, endogenous sPLA$_2$-X was spatiotemporally expressed in the anagen hair follicles of mouse skin, and the skin of *Pla2g10*-deficient mice had abnormal hair follicles with reduced hair growth and hypoplasic ORS. Thus, our results highlight a novel role of sPLA$_2$-X in hair homeostasis within a highly restricted and specialized skin compartment, the hair follicle.

EXPERIMENTAL PROCEDURES

Animals—All procedures involving animals were approved by the Institutional Animal Care and Use Committees of the Tokyo Metropolitan Institute of Medical Science and of Showa University in accordance with the Standards Relating to the Care and Management of Experimental Animals in Japan. The strategy for the generation and maintenance of Tg mice overexpressing *PLA2G10* under the β-actin promoter was reported previously (29). All the *PLA2G10*-Tg mice were inbred with C57BL/6 mice. Mice lacking sPLA$_2$-X (*Pla2g10*$^{-/-}$) (24) and phospholipase Cδ1 (*Plcd1*$^{-/-}$) (30) were described previously.

RT-PCR—Synthesis of cDNAs was performed using the High Capacity cDNA Reverse Transcription kit (Applied Biosystems). PCR reactions were carried out using GeneAmp Fast PCR system (Applied Biosystems) on the ABI9800 Fast Thermal Cycler (Applied Biosystems) with a primer pair that could amplify both mouse *Pla2g10* and human *PLA2G10* mRNAs (5′-GACGCCATTGACTGGTGCTGC-3′ and 5′-AGTTCTTG-GCATTTGTTCTCTGC-3′). For quantitative RT-PCR, PCR reactions were carried out using Power SYBR Green PCR system (Applied Biosystems) or TaqMan Gene Expression System (Applied Biosystems) on the ABI7700 Real Time PCR system (Applied Biosystems). The relative abundance of transcripts was normalized with constitutive expression of 18 S ribosomal RNA or β-actin mRNA. The oligonucleotide primers and probes (Roche Applied Science) used for quantitative RT-PCR are listed in supplemental Table S1.

Measurement of PLA$_2$ Activity—Tissues were soaked in 10 volumes of 20 mM Tris-HCl (pH 7.4) and then homogenized with a Polytron homogenizer. The homogenates were centrifuged at 10,000 × *g* for 10 min. PLA_2 activities in the supernatant were assayed by measuring the amounts of radiolabeled linoleic acid released from the substrate 1-palmitoyl-2-[^{14}C]linoleoyl-PE (PerkinElmer Life Sciences). The substrate in ethanol was dried under a stream of N_2 and dispersed in water by sonication. Each reaction mixture (total volume 250 μl) consisted of appropriate amounts of the required samples, 100 mM Tris-HCl (pH 7.4), 4 mM $CaCl_2$, and 1 μM substrate. After incubation for 30 min at 37 °C, [^{14}C]linoleic acid was extracted, and the radioactivity was quantified with a liquid scintillation counter as described previously (31). Protein contents were determined by BCA protein assay (Pierce).

Immunoprecipitation and Western Blotting—Rabbit polyclonal and mouse monoclonal anti-human sPLA$_2$-X antibodies were gifted from Dr. Michael Gelb (University of Washington, Seattle, WA) and Dr. Shinji Hatakeyama (Novartis Pharma, Tsukuba, Japan), respectively. Immunoprecipitation and immunoblotting were performed using these antibodies as described previously (32). In brief, a monoclonal antibody for human sPLA$_2$-X (7E2F11) or control mouse IgG_1 (2 mg) was conjugated with 0.5 ml of formyl cellurofine (Seikagaku Kogyo). The beads (20 μl) were incubated with 250 μl of skin homogenates obtained from *PLA2G10*-Tg or control mice at 4 °C overnight. After centrifugation, the beads were washed 5 times with 1 ml of PBS and boiled for 5 min in 20 μl of sodium SDS-PAGE sample buffer with β-mercaptoethanol. Then the resulting supernatants were applied to 12.5% SDS-PAGE gels, and sep-

arated proteins were transferred to nitrocellulose membranes. The membranes were subjected to immunoblotting with rabbit anti-human sPLA$_2$-X polyclonal antibody as described previously.

Histochemistry—Immunohistochemistry of mouse tissue sections was performed as described previously (33). In brief, skin samples were fixed with 100 mM phosphate buffer (pH 7.2) containing 4% paraformaldehyde and embedded in paraffin, sectioned, mounted on glass slides, deparaffinized in xylene, and rehydrated in ethanol with increasing concentrations of water. Hematoxylin and eosin staining was performed on 5-μm thick cryosections. For immunofluorescence, the tissue sections (5 μm) were incubated with 1× Blockace (DS Pharma BioMedical) in PBS for 30 min, washed 3 times with PBS for 5 min each, and incubated with rabbit antibody to mouse loricrin, filaggrin, cytokeratin 1, or cytokeratin 5 (Covance) at 1:1000–2000 dilution in 10× dilution of Blockace overnight at 4 °C. Sections were then washed 3 times with PBS for 5 min each and incubated with Alexa Fluor 647-labeled goat anti-rabbit IgG antibody (Molecular Probes) diluted to 1:1000 at 20 °C for 1 h. Counterstaining was performed with 4,6-diamino-2-phenylindole (DAPI) (Vector). Stained sections were analyzed with a confocal laser scanning microscope (LSM510 META, Carl Zeiss).

Electrospray Ionization Mass Spectrometry (ESI-MS)—Tissues were soaked in 10 volumes of 20 mM Tris-HCl (pH 7.4) and then homogenized with a Polytron homogenizer. Lipids were extracted from the homogenates by the method of Bligh and Dyer (34). The analysis was performed using a 4000Q-TRAP quadrupole-linear ion trap hybrid mass spectrometer (Applied Biosystems/MDS Sciex) with an Ultimate 3000 HPLC system (DIONEX Company) combined with an HTC PAL autosampler (CTC Analytics). The extracted lipids were subjected to electrospray ionization mass spectrometry analysis by flow injection (typically 3 nmol of phosphorus equivalent in the positive ion mode and 0.6 nmol of phosphorus equivalent in the negative ion mode) without liquid chromatography separation. The mobile phase composition was acetonitrile/methanol/water (6:7:2, v/v/v) (plus 0.1% ammonium formate (pH 6.8)) at a flow-rate of 10 μl/min. The scan range of the instrument was set at m/z 200–1000 at a scan speed of 1000 Da/s. The trap fill-time was set at 1 ms in the positive ion mode and at 20 ms in the negative ion mode. The ion spray voltage was set at 5500 V in the positive ion mode and at −4500 V in the negative ion mode. Nitrogen was used as curtain gas (setting of 10, arbitrary units) and as collision gas (set to "high"). The declustering potential was set at 100 V in the positive ion mode and at −100V in the negative ion mode. The collision energy in ESI-MS and ESI-MS/MS analyses were optimized according to the desired experiments. The method to detect the proper precursor ions and neutral losses derived from phospholipids in ESI-MS/MS analysis was described previously (35, 36).

For the assay of oxygenated lipids using LC-ESI-MS/MS analysis, tissues were soaked in ten volumes of methanol and then homogenized with a Polytron homogenizer. After overnight incubation at −20 °C, H_2O was added to the mixture to give a final methanol concentration of 10% (v/v). d_8-Labeled arachidonic acid (AA) (Cayman Chemicals) was added as an internal standard. The oxygenated lipids in the supernatant were extracted using Sep-Pak C18 cartridges (Waters). The LC-ESI-MS/MS analysis was performed using a 4000Q-TRAP quadrupole linear ion trap hybrid mass spectrometer (Applied Biosystems/MDS Sciex) with ACQUITY Ultra Performance LC® (Waters). The sample was applied to the ACQUITY UPLC™ BEH C18 column (1 × 150-mm inner diameter, 0.17-μm particle) and then to ESI-MS/MS analysis. The samples injected by the autosampler (10 μl) were directly introduced and separated by a step gradient with mobile phase A (water containing 0.1% (v/v) formic acid) and mobile phase B (acetonitrile:methanol = 4:1 v/v) at a flow rate of 50 μl/min and a column temperature of 30 °C. The specific detection of individual lipids was performed by multiple reaction monitoring (37).

Measurement of PGE$_2$—Tissues were soaked in 10 volumes of methanol and then homogenized with a Polytron homogenizer. After the homogenates were kept on −20 °C overnight, H_2O was added to the reaction mix (final concentration, 10% (v/v) methanol). The lipids were extracted by Sep-Pak C18 cartridges using [^{3}H]AA (GE Healthcare) as a calibrator of the sample recovery. After the columns were equilibrated with H_2O and methanol, the methanol extracts were applied to Sep-Pac C18 columns. The columns were sequentially washed with H_2O and then with hexane followed by elution of the bound lipids with methyl formate. The contents of PGE$_2$ in skin were quantified with a PGE$_2$ enzyme immunoassay kit (Cayman Chemical).

Microarray Gene Profiling—Total RNAs were isolated from the skin of *PLA2G10*-Tg and control mice (n = 4) or *Pla2g10*$^{+/+}$ and *Pla2g10*$^{-/-}$ mice (n = 4) at P25 by use of TRIzol reagent (Invitrogen) and purified using an RNeasy mini kit (Qiagen). cRNA targets were synthesized and hybridized with Whole Mouse Genome Oligo Microarray according to the manufacturer's instructions (Agilent). The array slides were scanned with a Laser Scanner GenePix 4000B (Molecular Devices) using appropriate gains on the photomultiplier to obtain the highest intensity without saturation. Gene expression values were background corrected and normalized using the GenePix software (Molecular Devices).

Microdissection—Mouse skin samples (P8) were embedded in OCT compound, sectioned (10-μm thick), mounted on a DIRECTOR LMD slide (AMR Inc.), fixed with cold ethanol/acetic acid (19:1, v/v) for 5 min, and stained with toluidine blue. Laser-capture microdissection was performed on cryosections using Leica LMD6000 system (Leica). mRNA was extracted using RNeasy Micro Kit (Qiagen) from the isolated hair follicle or epidermis fraction. Quantitative RT-PCR reactions were carried out using TaqMan Gene Expression system as described above.

For lipid analyses, lipids were extracted from the hair follicle or epidermis fraction microdissected from replicate skin sections without fixation with ethanol/acetic acid solution. An aliquot of the extracted lipids was subjected to PGE$_2$ enzyme immunoassay or to ESI-MS for quantification of phospholipids. The contents of PGE$_2$ in the microdissected samples were normalized with those of phospholipids as described previously (38).

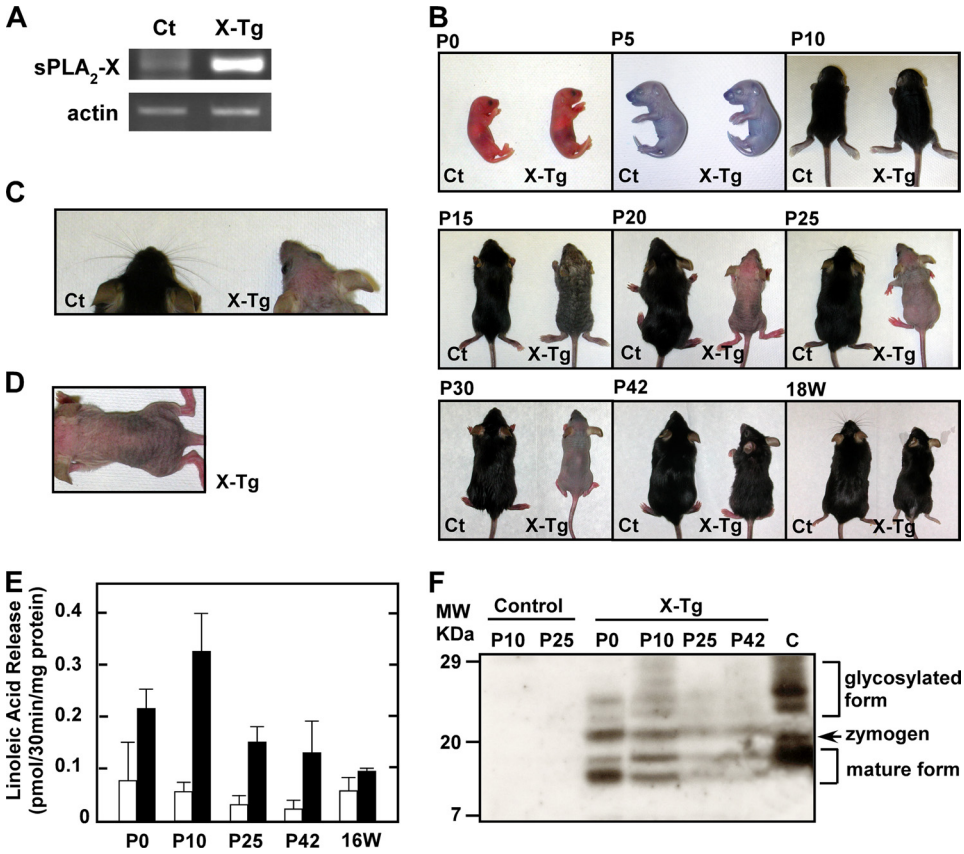

FIGURE 1. **Gross abnormality in the skin of *PLA2G10*-Tg mice.** *A*, shown is expression of sPLA$_2$-X in the skin of *PLA2G10*-Tg (*X-Tg*) and control (*Ct*) mice at P25, as assessed by RT-PCR. *B*, gross appearances of *X-Tg* and control littermates are shown. *X-Tg* mice were normal at birth (*P0*), and no gross abnormalities in coat hairs were apparent by P10. *X-Tg* mice began to lose coat hairs by P15 and were entirely bald over P20–P30. After this hairless period, new hairs reappeared in *PLA2G10*-Tg mice by P42. After 18 weeks, the fur of *X-Tg* mice looked matted, lusterless, coarse and ungroomed. *C*, a dorsal view of the head (whiskers) of control and *X-Tg* mice at P25 is shown. There were few whiskers on the Tg snout. *D*, shown is a dorsal view of the wrinkled skin of *X-Tg* mice at P20. *E*, PLA$_2$ enzymatic activity in homogenates of skin from control (*open columns*) and *X-Tg* (*solid columns*) mice at each postnatal point is shown. Data are the means ± S.D. ($n = 4$). *F*, detection of sPLA$_2$-X protein in skin homogenates by immunoblotting is shown. The homogenates from *X-Tg* and control mice at the indicated postnatal points were immunoprecipitated with mouse monoclonal anti-human sPLA$_2$-X antibody and immunoblotted with rabbit polyclonal anti-human sPLA$_2$-X antibody. Positions of mature, zymogen, and glycosylated forms of sPLA$_2$-X protein, as evaluated by comparison with a positive control (PC12 cells infected with adenovirus expressing sPLA$_2$-X (22)) (*C*), are indicated in the *right margin*.

Transmission Electron Microscopy—Mouse skin was fixed with 1% glutaraldehyde, 4% paraformaldehyde, and 0.1 M phosphate buffer (pH 7.4) at 4 °C overnight. After a brief wash with PBS, post-fixation with 2% OsO_4^- in PBS was carried out for 1 h followed by gradual dehydration with ethanol. The skin was embedded in Poly/Bed812 EPON (Polyscience). Thin serial sections (100-nm thick) were stained with uranyl acetate and lead acetate. Ultrastructures of the samples were examined at 80 kV with a JEM-1010 (Jeol Ltd.).

Statistics—Data were statistically evaluated by unpaired Student's *t* test at a significance level of $p < 0.05$.

RESULTS

Development of Alopecia in PLA2G10-Tg Mice—We previously established *PLA2G10*-Tg mice, in which the majority of overexpressed sPLA$_2$-X protein existed as an inactive zymogen in most tissues (29). RT-PCR of dorsal skin from control and Tg mice at postnatal day 25 (P25) revealed that mRNA for sPLA$_2$-X was endogenously expressed in control skin at a trace level (for details, see below), and it was markedly increased in Tg skin (Fig. 1*A*). Although *PLA2G10*-Tg mice appeared normal up to postnatal day 10 (Fig. 1*B* (*P10*)), complete loss of coat hairs was observed at 20–30 days (Fig. 1*B* (*P20-P30*)). Most Tg pups also had no or few whiskers (Fig. 1*C*), and their bald skin was wrinkled (Fig. 1, *B* (*P20-P30*) and *D*). After this hairless period, new pelage hairs appeared by P42 and were sustained for more than 1 year. After 18 weeks of age, however, the fur of *PLA2G10*-Tg mice appeared matted, lusterless, coarse, and ungroomed (Fig. 1*B* (*18W*)). Some older mice began to show thinning fur and small patchy areas of hair loss, particularly between the ears and on the back, where epidermal thickening was histologically obvious (data not shown). No apparent histological abnormality was found in various tissues of *PLA2G10*-Tg mice as they aged, including lung, liver, kidney, heart, small intestine, and colon (supplemental Fig. S1). Nevertheless, because the severe skin abnormalities in *PLA2G10*-Tg mice were particularly evident during P15-P30, in subsequent studies we focused on detailed phenotypic analyses of Tg mouse skin at this early stage.

The remarkable skin-specific phenotype of *PLA2G10*-Tg mice during the early period of life suggests that the proteolytic activation of sPLA$_2$-X should have temporally occurred in the skin. In fact, a PLA$_2$ enzymatic assay conducted using 1-palmitoyl-2-linoleoyl-PE as a substrate demonstrated that the activ-

ity in *PLA2G10*-Tg skin was increased 3- and 6-fold relative to that in control skin (reflecting the combined activities of various intrinsically present PLA$_2$ enzymes) at P0 and P10, respectively (Fig. 1*E*). After reaching a peak value around P10, the PLA$_2$ activity in Tg skin declined gradually to a level only <2-fold higher than that in control skin by 16 weeks. When skin homogenates were immunoprecipitated with mouse anti-human sPLA$_2$-X monoclonal antibody followed by immunoblotting with rabbit anti-human sPLA$_2$-X polyclonal antibody, three major bands with molecular masses of 11, 14, and 20 kDa as well as broad 21~29-kDa bands were detected in *PLA2G10*-Tg skin, whereas they were undetectable in control skin (because mouse monoclonal anti-human sPLA$_2$-X antibody failed to pull down endogenous mouse sPLA$_2$-X) (Fig. 1*F*). Overall, the expression of immunoreactive sPLA$_2$-X proteins in Tg skin was higher during P0–P10 than during P25–42 (Fig. 1*F*). As evaluated from the molecular sizes of authentic mature, zymogen and glycosylated forms of sPLA$_2$-X (sPLA$_2$-X overexpressed in PC12 cells (22); *lane C* in Fig. 1*F*), the 14-kDa species, whose intensity paralleled the PLA$_2$ activity (Fig. 1*E*), appeared to correspond to the mature sPLA$_2$-X. The smallest 11-kDa band might have been a cleaved fragment of sPLA$_2$-X, although its precise identity requires further clarification. Nevertheless, the data for PLA$_2$ activity (Fig. 1*E*) and immunoblotting (Fig. 1*F*) indicate that the mature (active) form of sPLA$_2$-X was produced during a period when skin abnormality became evident in the Tg mice (see below).

PLA2G10-Tg Mice Display Unusual Hair Cycling, Hair Distortion, and Epidermal Hyperplasia—In mice, initial development of hair follicles starts from E13 to E18 and extends to P14 (growing phase or anagen) (1–3). Hematoxylin/eosin-stained sections of the mid-dorsal skin of newborn (P0) *PLA2G10*-Tg mice appeared entirely normal (supplemental Fig. S2). At P5, when wild-type follicles were in anagen, all follicular cell types were present, and the follicles had penetrated into the adipose layer, whereas fewer follicles could be found in the deeper regions of subcutaneous fat tissue in Tg mice. At P10, almost all pelage hair follicles of control mice had entered the final stage of anagen morphogenesis, having acquired their maximal length with hair shafts that had broken through the epidermis. Notably, many hair follicles in the skin of age-matched Tg mice had already entered catagen (regression phase), when retracting epithelial hair shafts had separated from the dermal papilla, indicating precocious entry of the Tg hair follicles into the growth-resting transition stage of the first postnatal hair growth cycle. Thereafter, hair follicles in control mice were synchronized in catagen at P15, telogen (resting phase) at P20, and transition from telogen to the next (second) anagen at P25 (1–3), whereas the majority of hair follicles in *PLA2G10*-Tg mice were still in telogen at P25. Moreover, although hair follicles in control skin were entirely in anagen at P30–P42, follicles exhibiting the telogen feature still existed in Tg skin, suggesting delayed transition of the Tg follicles to the next anagen. Thus, the effects of Tg expression of sPLA$_2$-X culminate in abnormal hair cycling, with shortened anagen and prolonged catagen and telogen.

The dorsal skin of *PLA2G10*-Tg mice at P10–42, in which alopecia had developed (Fig. 1*B*), exhibited an abnormal hair

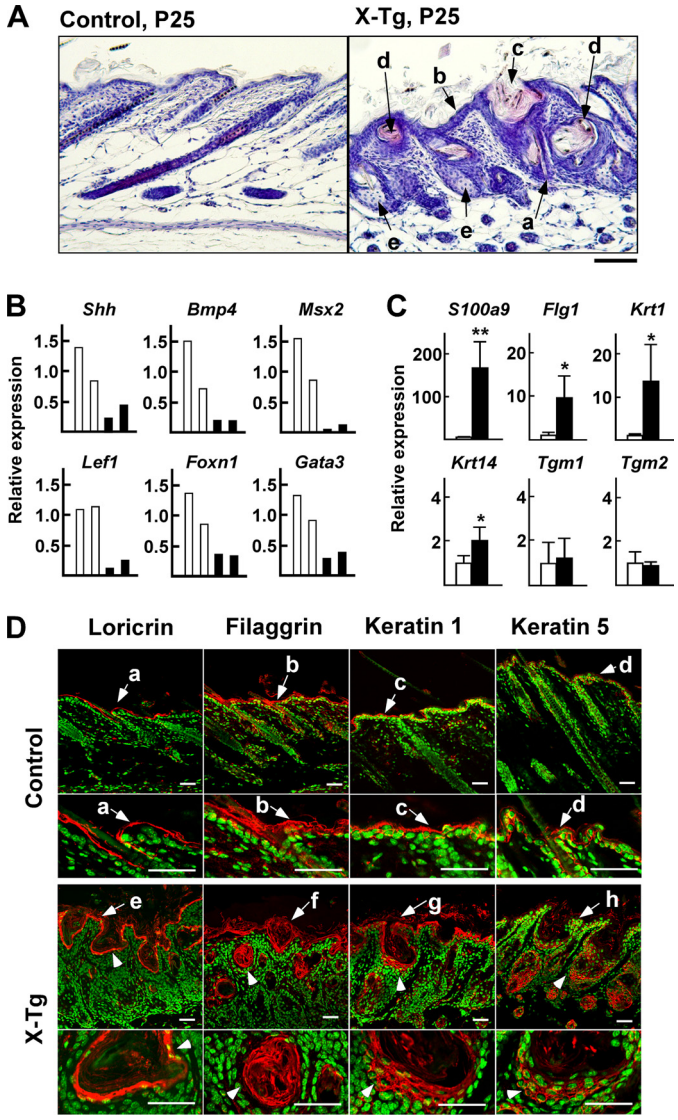

FIGURE 2. **Hair follicle distortion, epidermal hyperplasia with hyperkeratosis, and sebaceous gland enlargement in the skin of *PLA2G10*-Tg mice.** *A*, sections from control and *PLA2G10*-Tg (*X-Tg*) mice at P25 were stained with hematoxylin and eosin. In the Tg mice, the hair shafts appeared thin and distorted (*arrow a*); epidermal thickening (*arrow b*) and enlarged hair follicles (*arrow c*) were obvious; some follicles had degenerated into cyst-like structures filled with keratinized debris and surrounded by multilayered epithelium (*arrow d*); sebaceous glands displayed hyperplasia (*arrow e*). *B* and *C*, expression of genes associated with the differentiation of hair follicles and hair shafts (*B*) and of the interfollicular epidermis (*C*) in the skins of *PLA2G10*-Tg mice (*solid columns*) and control mice (*open columns*) at P25 was assessed by quantitative RT-PCR. Data are two representative results for each genotype (*B*) and means ± S.D. ($n = 4$; *, $p < 0.05$; **, $p < 0.01$) (*C*). The expression levels of individual genes in control mice are regarded as 1, with the expression of ribosomal RNA (18 S) as a reference. *D*, confocal laser scanning microscopy of various epidermal differentiation markers in dorsal skins from control and *X-Tg* mice at P25 is shown. Individual markers were stained *red* with specific antibodies, and nuclei were stained *green* with DAPI. Loricrin was present in the cornified layers (*arrows a* and *e*), filaggrin in the cornified and granular layers (*arrows b* and *f*), keratin 1 in the granular and spinous layers (*arrows c* and *g*), and keratin 5 in a single basal layer (*arrows d* and *h*). In *X-Tg* mice, loricrin-, filaggrin-, keratin 1-, and keratin 5-positive signals were distributed in the cysts (*arrowheads*). *Bars* represent 20 μm for all panels.

follicle and epidermal histology (Fig. 2*A* and supplemental Fig. S2). The most obvious changes were fragile hairs (Fig. 2*A*, *a*), epidermal thickening (Fig. 2*A*, *b*), and enlarged hair follicles (Fig. 2*A*, *c*), which were already apparent at P15 and manifested

at P25. Follicular enlargement appeared to result primarily from thickened ORS. At P25, some follicles had degenerated into cyst-like structures filled with keratinized debris and surrounded by multilayered epithelium (Fig. 2*A*, *d*). Both the squamous and suprabasal cellular layers, which appeared overall to be irregular and disorganized, contributed to the dramatic epidermal thickening. In *PLA2G10*-Tg mice, the uppermost layers of the epidermis displayed hyperkeratosis with a highly thickened stratum corneum, and hair shafts appeared thin, fragile, and often distorted. In addition, the sebaceous glands, an epidermal appendage budding from the upper ORS, of Tg mice displayed hyperplasia, which was characterized by the presence of numerous lobules consisting of sebocytes grouped around an enlarged sebaceous gland duct (Fig. 2*A*, *e*). In contrast, dermal infiltration of inflammatory cells and epidermal erosions, which are commonly observed in patients with inflammatory skin diseases such as psoriasis and atopic dermatitis, were scarcely evident in *PLA2G10*-Tg mice.

The histochemical data presented above indicate that overexpression of sPLA$_2$-X *in vivo* leads to abnormal hair differentiation with perturbed hair cycling in the skin niche. To gain further molecular insight into these changes, we carried out quantitative RT-PCR with skin from *PLA2G10*-Tg mice and littermate controls at P25 (Fig. 2, *B* and *C*). In line with the hairless phenotype of *PLA2G10*-Tg mice, quantitative RT-PCR revealed markedly reduced expression of a subset of genes related to hair follicle differentiation and hair shaft formation, such as *Shh* (Sonic Hedgehog) and *Bmp4* (bone morphogenetic protein 4), which regulate the proliferation and differentiation of matrix cells in the dermal papilla, and *Msx2*, *Lef1*, *Foxn1*, and *Gata3*, which are transcription factors required for proper differentiation of the hair shaft or IRS (1–3) (Fig. 2*B*). Quantitative RT-PCR analyses also showed marked increases ($> \sim$ 10-fold) in several mRNAs that could account for accelerated terminal differentiation of epidermal keratinocytes (Fig. 2*C*). These included mRNA for *S100a9* (S100 family protein A; S100A), *Flg1* (filaggrin 1), and *Krt1* (keratin 1), which are enriched in the well differentiated stratum corneum and granulosum layers (2, 39). A moderate increase in *Krt14* (keratin 14), a basal layer keratin (2, 39), was also notable, whereas the expression of *Tgm1* (transglutaminase 1) and *Tgm2*, which are expressed in the stratum spinosum and basale (2, 39), did not differ appreciably between *PLA2G10*-Tg and control mice (Fig. 2*C*).

To verify whether the changes in these epidermal genes would be histologically relevant, we stained skin sections with antibodies for epidermal differentiation markers (2, 39). As expected, loricrin was present in the cornified layer (Fig. 2*D*, *a*), filaggrin in the cornified and granular layers (Fig. 2*D*, *b*), keratin 1 in the granular and spinous layers (Fig. 2*D*, *c*), and keratin 5 in a single basal layer (Fig. 2*D*, *d*) in the skin of control mice. Consistent with the quantitative RT-PCR analyses, increases in loricrin (Fig. 2*D*, *e*)-, filaggrin (Fig. 2*D*, *f*)-, keratin 1 (Fig. 2*D*, *g*)-, and keratin 5 (Fig. 2*D*, *h*)-positive cells were obvious in the epidermis of *PLA2G10*-Tg mice. Staining of keratin 5 extended focally to the upper epidermal layers as well as to the thickened hair follicular epidermal layers, and thickening of the loricrin-, filaggrin- and even keratin 1-positive signals in the stratum corneum was evident (Fig. 2*D*, *e-g*). Moreover, positive signals for these differentiation markers were also distributed in the cysts; loricrin and filaggrin were located in the innermost cell layers as well as in the keratinized debris within the cysts, and staining of keratin 1 and keratin 5 was positive in multiple layers of cells surrounding the cysts (Fig. 2*D*, *arrowhead*). These results indicate that the cysts resulted from abnormal and mis-directional (inward) differentiation of epidermal keratinocytes in *PLA2G10*-Tg skin.

Hair and epidermal abnormalities are often associated with dysregulated balance of proteases and protease inhibitors (40–48). Indeed, quantitative RT-PCR showed that the expression levels of *Klk6* (kallikrein 6), *Klk7* (kallikrein 7), and *Ctsl* (cathepsin L), but not *Klk8* (kallikrein 8), *Mstp1* (matriptase/MT-SP1), and *furin* (a subtilisin family protease), were increased significantly in *PLA2G10*-Tg skin relative to control skin (supplemental Fig. S3*A*). Considering that the amino acid sequence of the N-terminal cleavage site in sPLA$_2$-X is similar to that cleaved by kallikreins or cathepsins (49), these inducible proteases identified thus far might contribute to the proteolytic activation of sPLA$_2$-X in Tg skin. It was also noted that expression of the cysteine protease inhibitor *Cst6* (cystatin M/E) and the serine protease inhibitor *Spink5/Lekt1*, abnormalities of which are associated with ichthyosis (46, 47), was increased 22.8- and 2.6-fold, respectively, in *PLA2G10*-Tg skin relative to control skin (supplemental Fig. S3*B*). These changes also reflect the hair and epidermal abnormalities in Tg mice.

Lipid Analysis of PLA2G10-Tg Skin—To identify the *in vivo* hydrolytic action of sPLA$_2$-X on phospholipids, we next carried out ESI-MS/MS analysis of phospholipids using skin from *PLA2G10*-Tg mice and littermate controls at P25. Precursor ion scanning of choline-containing phospholipid molecular species revealed that the skin from control mice contained PC species mainly with C16:0-C16:0 (32:0), C16:0-C18:1 (34:1), and C18:0-C18:2 (36:2) (Fig. 3*A*, *right panel*) and trace levels of lysophosphatidylcholine species with C16:0 and C18:0 (Fig. 3*A*, *left panel*). Although sPLA$_2$-X is the most potent sPLA$_2$ isoform capable of acting on PC-rich membranes (21), none of these PC and lysophosphatidylcholine molecules was changed appreciably in *PLA2G10*-Tg mice in comparison with control mice. In contrast, neutral loss scanning of ethanolamine-containing phospholipid molecular species demonstrated that, of the major PE species (C18:0-C18:2 (36:2), C18:0-C20:4 (38:4), C18:1-C20:5 (38:6), and C18:0-C22:6 (40:6)), those with C18:0-C20:4 (38:4), C18:1-C20:5 (38:6), and C18:0-C22:6 (40:6) were reduced by ~50% in the skin of *PLA2G10*-Tg mice relative to that of controls (Fig. 3*B*, *right panel*). The marked reduction of these PE species was accompanied by a concomitant increase in C18:0 and C18:1 lysophosphatidylethanolamine species (Fig. 3*B*, *left panel*). The compositions of phosphatidylserine and phosphatidylinositol did not differ between the genotypes (supplemental Fig. S4). Thus, sPLA$_2$-X overexpressed in mouse skin preferentially hydrolyzed PE with polyunsaturated fatty acid (PUFA), including AA (C20:4), eicosapentaenoic acid (C20:5), and docosahexaenoic acid (C22:6).

We next performed LC-ESI-MS/MS analysis that was optimized for semiquantitative detection of various PUFAs and their oxygenated products (37). Consistent with the changes in PUFA-containing PE species, levels of free AA, eicosapen-

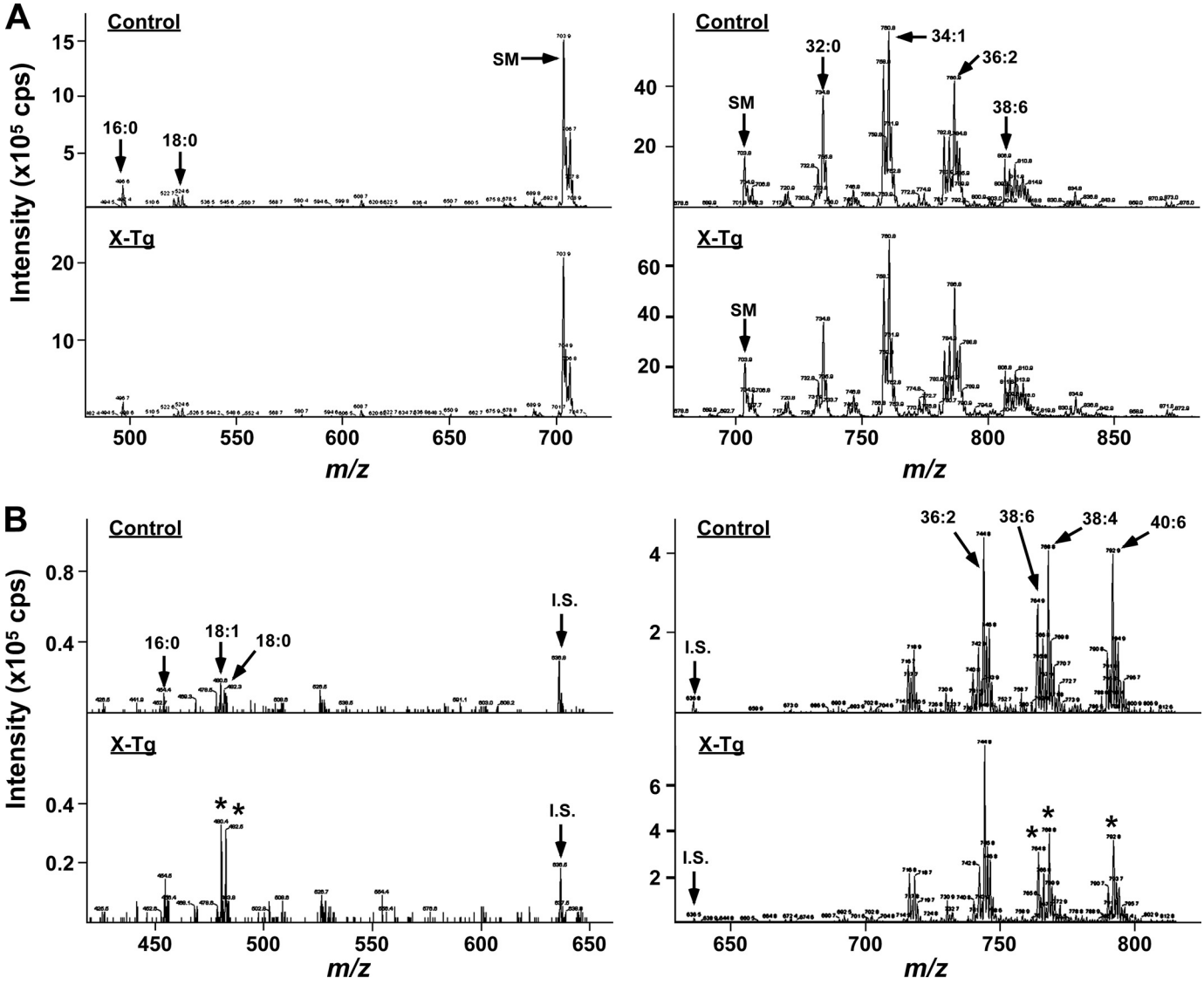

FIGURE 3. **Hydrolysis of skin phospholipids in *PLA2G10*-Tg skin.** Lipids were extracted from the skin of *PLA2G10*-Tg (*X-Tg*; *lower panels*) and control (*upper panels*) mice at P25 and subjected to ESI-MS (see "Experimental Procedures"). Precursor ion scanning of lysophosphatidylcholine (*m/z*: 400–710; *left panel*) and PC (*m/z*: 670–880; *right panel*) (*A*) and neutral loss scanning of lysophosphatidylethanolamine (*m/z*: 450–650; *left panel*) and PE (*m/z*: 700–810; *right panel*) (*B*) molecular species were performed. Peaks for major molecular species, sphingomyelin (d18:1–16:0) (*SM*), and the internal standard (*i.s.*: C14:0-C14:0 PE) are indicated. Representative results of four independent experiments are shown. *Asterisks* indicate the peaks that were markedly altered in *X-Tg* mice compared with control mice.

taenoic acid, and docosahexaenoic acid were nearly doubled in Tg mice relative to control mice (Fig. 4*A*). Of the AA metabolites detected so far, the levels of PGE_2 and PGI_2 (6-keto-$PGF_{1\alpha}$ as a stable end-product) were increased substantially, those of PGD_2 and 12- and 15-HETEs were unchanged, and those of 5- and 8-HETEs were decreased in the skin of *PLA2G10*-Tg mice relative to the controls (Fig. 4*B*). The increased amount of PGE_2 in *PLA2G10*-Tg skin relative to control skin was confirmed by PGE_2 enzyme immunoassay (Fig. 4*C*), thus validating the LC-ESI-MS/MS approach.

Because the profile of eicosanoids can be determined not only by the supply of free AA by PLA_2s but also by the actions of downstream biosynthetic enzymes, we examined whether or not the expression of COXs, lipoxygenases (LOXs), and terminal synthases would be altered in *PLA2G10*-Tg skin. Quantitative RT-PCR showed 2~3-fold increases in the expression levels of COX-1 (*Ptgs1*) and microsomal PGE synthase-1 (mPGES-1) (*Ptges*) in *PLA2G10*-Tg skin compared with control skin, whereas the expression levels of COX-2 (*Ptgs2*) and two other PGE synthases (*Ptges2* and *Ptges3*) were unchanged (Fig. 4*D*), suggesting that the increased PGE_2 production in *PLA2G10*-Tg skin (Fig. 4, *B* and *C*) may be derived mainly from the COX-1/mPGES-1 pathway. The expression levels of epidermal LOXs, including epidermal 12-LOX (*Alox12e*) and 12R-LOX (*Alox12b*), abnormalities of which have been shown to be associated with epidermal disorders (50, 51), were higher in *PLA2G10*-Tg skin than in control skin (Fig. 4*E*), consistent with the epidermal hyperplasia in Tg mice. Expression of 5-LOX (*Alox5*), an LOX isozyme responsible for leukotriene synthesis, was low, in agreement with the poor leukocyte infiltration (see above) and low 5-HETE production (Fig. 4*B*) in Tg skin.

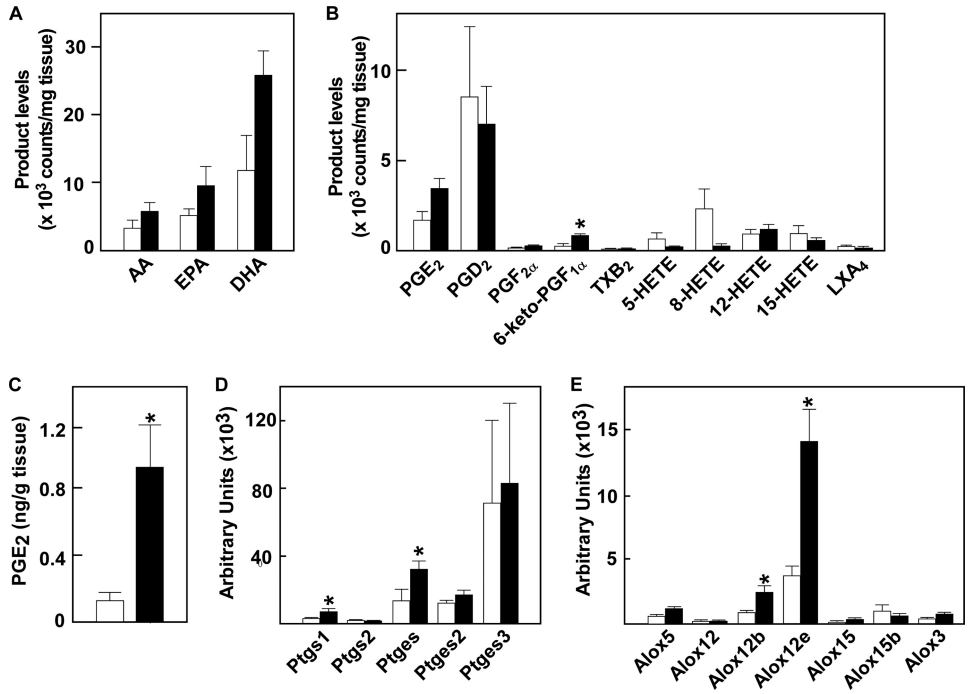

FIGURE 4. **Altered lipid mediator profiles in the skin of *PLA2G10*-Tg mice.** Lipids were extracted from skins of *PLA2G10*-Tg (*solid columns*) and control (*open columns*) mice at P25 and subjected to LC-ESI-MS/MS (see "Experimental Procedures"). *A* and *B*, signal intensities for AA, eicosapentaenoic acid (*EPA*), docosahexaenoic acid (*DHA*; *A*), and AA metabolites (*B*) were counted and normalized with an internal control (d_8-labeled AA). TXB_2, thromboxane B_2; *LXA_4*, lipoxin A_4. *C*, PGE_2 in the skin was quantified by enzyme immunoassay. Data are the mean ± S.E. ($n = 4$). *D*, expression of the genes related to PGE_2 synthesis in the skins of *PLA2G10*-Tg mice (*solid columns*) and control mice (*open columns*) at P25 are shown. *E*, expression of genes related to the lipoxygenase pathways in the skin of *PLA2G10*-Tg mice (*solid columns*) and control mice (*open columns*) at P25 is shown. Data are the means ± S.D. ($n = 4$). In *D* and *E*, the expression levels of individual genes were normalized with the expression of ribosomal RNA (18 S).

Gene Expression Microarray Profiling of PLA2G10-Tg Skin—Microarray gene profiling of skin from *PLA2G10*-Tg mice in comparison with that from control mice yielded further supportive data for explaining the overall tendency of Tg skin to show hair follicle distortion and epidermal hyperplasia associated with hyperkeratosis in the absence of inflammation (Fig. 5 and supplemental Table S2). In agreement with the histologic and quantitative RT-PCR data (Fig. 2), microarray analysis showed markedly increased expression of genes that are enriched in the well differentiated stratum corneum and granulosum layers (*e.g. S100a9*, *Lor*, *Sprr*, *Flg1*, *Krt1*, and *Krt10*), moderate increases of basal keratins (*e.g. Krt5* and *Krt14*), and minimal changes in the expression of genes associated with the stratum spinosum and basale (*e.g. Tgm*, *Dsg*, and *Lama5*) in *PLA2G10*-Tg mice (Fig. 5), thus accounting for the accelerated terminal differentiation of epidermal keratinocytes. Furthermore, in line with the hairless phenotype, the expression of genes involved in differentiation of hair follicles and hair shafts (*e.g. Shh*, *Bmp4*, *Msx2*, *Lef1*, *Foxn1*, *HoxC13*, and *Gata3*) as well as those for various hair keratins and hair keratin-associated proteins was dramatically decreased in *PLA2G10*-Tg skin relative to control skin (Fig. 5). In addition, the expression of a subset of genes for transcription factors that have been implicated in hair germ cell fate at the bulge (*e.g. Ctnnb1*, *Tcf3*, and *Lhx2*) was substantially lower in *PLA2G10*-Tg skin than in control skin. Finally, in agreement with the histological absence of inflammatory cells in the skin of *PLA2G10*-Tg mice (see above), neither microarray gene profiling (supplemental Table S2) nor quantitative RT-PCR (data not shown) revealed significant expression of proinflammatory cytokines, such as *Il1b*, *Il4*, *Il6*, *Il12a*, *Il12b*, *Ifng*, and *Tnf* (4, 5), in *PLA2G10*-Tg skin. Expression of a limited group of cytokines and chemokines reported to participate in skin biology, such as *Il18*, *Ccl19*, *Ccl21*, *Ccl27*, *Cxcl14*, and *Cxcl16* (4, 5), showed substantial changes in *PLA2G10*-Tg skin relative to control skin (supplemental Table S2).

Endogenous sPLA$_2$-X Is Spatiotemporally Expressed in Hair Follicles—On the basis of the aforementioned results, we speculated that endogenous sPLA$_2$-X would be expressed somewhere in mouse skin, whose homeostasis is hampered by overexpression of this enzyme. However, expression of endogenous *Pla2g10* mRNA in whole mouse skin was only at a trace level (Fig. 1*A*), and we did not observe apparent abnormality in the gross appearance of coat hairs in *Pla2g10*$^{-/-}$ mice (data not shown). To determine any detectable changes in the skin of *Pla2g10*$^{-/-}$ mice, we attempted to compare overall gene expression in *Pla2g10*$^{-/-}$ skin with that in *Pla2g10*$^{+/+}$ skin by microarray gene profiling. We found that the expression levels of a panel of genes for hair keratins and hair keratin-associated proteins in the hair shaft were decreased 2~3-fold in *Pla2g10*$^{-/-}$ skin compared with *Pla2g10*$^{+/+}$ skin (Fig. 5). Expression of genes encoding several transcription factors for hair-associated genes, such as *Foxn1*, *Hoxc13*, *Lef1*, and *Msx2*, was also consistently lower in *Pla2g10*$^{-/-}$ skin than in *Pla2g10*$^{+/+}$ skin. In contrast, expression of genes for the dermal papilla, hair germ, and epidermis as well as those related to inflammation (cytokines and chemokines) was mostly unaltered in *Pla2g10*$^{-/-}$ skin (Fig. 5 and supplemental Table S2).

Distribution		Genes	Accession No	Signal intensities			Signal intensities		
				Ct	Tg	Tg/Ct	WT	KO	KO/WT
Epidermis	Terminal differentiation of epidermal keratinocytes	S100a9	NM_009114	59	5947	100.80	107	85	0.79
		Lor	NM_008508	32866	53029	1.61	38691	44315	1.15
		Ivl	NM_008412	170	390	2.29	162	151	0.93
		Filaggrin	LOC675741	657	4693	7.14	1416	1142	0.81
		Krt1	NM_008473	1650	17019	10.32	1105	1373	1.24
		Krt10	NM_010660	31463	53869	1.71	27230	34936	1.28
	Stratum spinosum and basale	Krt5	NM_027011	40018	52235	1.31	22791	27064	1.19
		Krt14	NM_016958	14820	27570	1.86	8940	9376	1.05
		Lama5	XM_203796	1121	720	0.64	657	618	0.94
		Tgm1	NM_019984	752	880	1.17	547	407	0.74
		Tgm2	NM_009373	1285	1141	0.89	667	863	1.29
		Dsg1a	AK029294	618	788	1.28	516	541	1.05
		Dsg2	BC034056	158	143	0.91	107	91	0.85
Hair follicle	Stem cells	Ctnnb1	NM_007614	2707	2121	0.78	1734	1524	0.88
		Lhx2	NM_010710	3431	2212	0.65	1880	2457	1.31
		Tcf3	NM_009332	864	608	0.70	385	402	1.04
		Tcf4	NM_013685	718	849	1.18	564	637	1.13
		Mki67	X82786	5454	3504	0.64	2758	2698	0.98
	Hair follicle differentiation and hair shaft differentiation	Shh	NM_009170	171	88	0.52	73	74	1.01
		Bmp4	NM_007554	316	191	0.60	194	171	0.88
		Gata3	NM_008091	2676	1396	0.52	1478	1523	1.03
		Msx2	NM_013601	768	279	0.36	479	288	0.60
		Lef1	NM_010703	1064	305	0.29	477	339	0.71
		Foxn1	NM_008238	152	72	0.47	94	64	0.68
		Hoxc13	NM_010464	78	30	0.39	54	32	0.59
	Hair keratin	Krt16	NM_008470	353	3487	9.88	250	250	1.00
		Krt6a	NM_008476	617	923	1.50	369	326	0.88
		Krt6b	NM_010669	151	272	1.80	121	94	0.78
		Krt17	NM_010663	22175	25433	1.15	13256	13294	1.00
		Krt19	NM_008471	79	77	0.98	52	42	0.81
		Krt75	NM_133357	14477	5638	0.39	7901	5976	0.76
		Krt31	NM_010659	1840	444	0.24	1579	659	0.42
		Krt33a	NM_027983	6322	1159	0.18	7864	3303	0.42
		Krt33b	XM_126759	4817	679	0.14	5868	2161	0.37
		Krt34	NM_027563	2960	541	0.18	4249	1677	0.40
		Krt36	XM_618928	403	132	0.33	217	118	0.54
		Krt83	NM_001003668	1924	406	0.21	2639	1125	0.43
		Krt86	NM_010667	3208	684	0.21	3558	1442	0.41
		Krt32	NM_010665	1398	515	0.37	1169	547	0.47
		Krt35	NM_016880	27089	7930	0.29	10767	6393	0.59
		Krt82	NM_053249	192	65	0.34	179	74	0.41
		Krt84	NM_008474	73	29	0.40	71	35	0.49
		Krt85	NM_016879	2157	775	0.36	1728	1034	0.60
		Krt13	NM_010662	2454	2819	1.15	1842	1629	0.88
		Krt18	NM_010664	97	37	0.38	85	36	0.42
		Krt71	NM_019956	39149	15050	0.38	29298	16989	0.58
		Krt25	NM_133730	35952	11169	0.31	21528	11960	0.56
		Krt27	NM_010666	16214	6925	0.43	14463	8411	0.58
		Krt8	NM_031170	108	42	0.39	59	35	0.59
		Krt15	NM_008469	17359	14552	0.84	11120	16799	1.51
	Keratin associated protein	Krtap2-4	BY717254	80	33	0.41	139	69	0.50
		Krtap3-1	XM_894811	1231	237	0.19	1919	807	0.42
		Krtap3-2	NM_025720	304	80	0.26	500	287	0.57
		Krtap3-3	NM_025524	157	35	0.22	275	113	0.41
		Krtap4-7	NM_029613	582	134	0.23	710	327	0.46
		Krtap5-1	NM_015808	2118	439	0.21	3884	1266	0.33
		Krtap5-2	NM_027844	231	73	0.32	320	112	0.35
		Krtap5-4	NM_015809	2759	599	0.22	4593	1481	0.32
		Krtap6-1	NM_010672	1900	143	0.08	4160	1428	0.34
		Krtap6-2	NM_010673	104	18	0.17	235	82	0.35
		Krtap6-3	D89901	3319	423	0.13	6158	2136	0.35
		Krtap8-1	AK133727	1191	201	0.17	1400	530	0.38
		Krtap8-2	NM_010676	1194	325	0.27	1420	666	0.47
		Krtap9-1	NM_015741	316	116	0.37	576	299	0.52
		Krtap12-1	NM_010670	117	29	0.25	204	50	0.25
		Krtap13-1	NM_183189	442	192	0.43	606	241	0.40
		Krtap14	NM_013707	555	42	0.08	751	216	0.29
		Krtap15	NM_013713	50	16	0.32	89	32	0.36
		Krtap16-1	NM_130870	255	19	0.08	803	250	0.31
		Krtap16-4	NM_130873	276	18	0.07	763	197	0.26
		Krtap16-5	NM_130857	287	26	0.09	639	225	0.35
		Krtap16-7	NM_130875	636	74	0.12	1248	424	0.34
		Krtap16-8	NM_130856	924	41	0.04	1777	666	0.38
		Krtap16-9	NM_130876	1742	53	0.03	3771	1084	0.29
		Krtap16-10	NM_183296	3375	104	0.03	6041	1727	0.29

:>2.0 :>1.5 :<0.75 :<0.50

FIGURE 5. **Microarray analyses of skins from *PLA2G10*-Tg and *Pla2g10*$^{-/-}$ mice in comparison with control mice.** Total RNAs were isolated from skins of *PLA2G10*-Tg (*Tg*) and control mice (*Ct*) or *Pla2g10*$^{+/+}$ (*Wt*) and *Pla2g10*$^{-/-}$ (*KO*) mice at P25 ($n = 4$). Equal amounts of RNA (pooled from four mice for each genotype) were subjected to gene expression microarray, as described under "Experimental Procedures." A representative result of two independent and reproducible experiments is shown. Fluorescent intensity values and their ratios (*Tg/Ct* or *Ko/Wt*) are shown. Individual genes were sorted into groups corresponding to epidermal and hair follicular components.

These results suggest that *Pla2g10*$^{-/-}$ mice may have some abnormalities in hair follicles but not in other skin compartments including epidermis, dermis, and sebaceous glands.

Several previous studies have reported that sPLA$_2$-X is expressed in epidermal keratinocytes of human and mouse skins (52, 53). However, despite considerable effort, we were unable to detect sPLA$_2$-X in mouse epidermis. Although we performed immunohistochemistry using five distinct anti-sPLA$_2$-X antibodies, none of them showed epidermal localization of sPLA$_2$-X at P0. Indeed, all of the antibodies used so far stained the epidermis of both *Pla2g10*$^{+/+}$ and *Pla2g10*$^{-/-}$ mice equally (Fig. 6*A*), indicating that the epidermal staining was

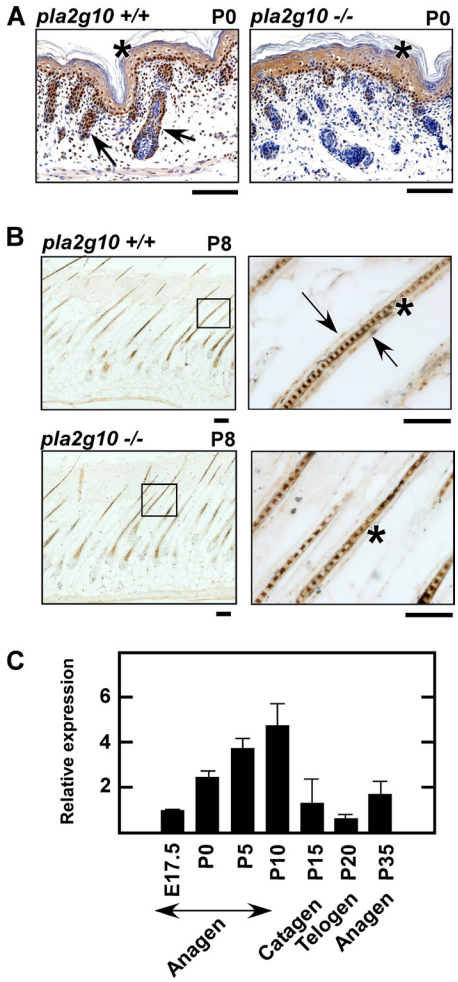

FIGURE 6. **Localization of endogenous sPLA$_2$-X in hair follicles.** *A* and *B*, immunohistochemistry of sPLA$_2$-X in skin sections from *Pla2g10*$^{+/+}$ and *Pla2g10*$^{-/-}$ mice at the newborn (P0) (*A*) and mid-anagen (P8) (*B*) stages using an anti-sPLA$_2$-X antibody is shown. *Boxed areas* are magnified in the *right panels* (*B*). Specific staining for sPLA$_2$-X was associated with the ORS in hair follicles (*arrows*) of *Pla2g10*$^{+/+}$ but not *Pla2g10*$^{-/-}$ mice. Nonspecific staining (*i.e.* seen in both *Pla2g10*$^{+/+}$ and *Pla2g10*$^{-/-}$ mice) of the epidermis (*A*) and hair shaft (*B*) is shown by *asterisks*. *Bars*, 100 μm. *C*, shown is quantitative RT-PCR analysis of the developmental expression of *Pla2g10* mRNA in the skin of C57BL/6 mice. Expression of *Pla2g10* at E17.5 relative to that of the housekeeping gene *Gapdh* is regarded as 1. Data are the mean ± S.E. (n = 5).

nonspecific. We noticed that, besides this pseudo-positive epidermal staining, sPLA$_2$-X immunoreactivity was distributed in hair follicles of wild-type but not knock-out skin at P0 (Fig. 6*A*). Hair follicles appeared smaller in *Pla2g10*$^{-/-}$ mice than in *Pla2g10*$^{+/+}$ mice (Fig. 6*A*), in agreement with the microarray results (Fig. 5). At P8 (mid-anagen), sPLA$_2$-X immunoreactivity was localized in the outermost layer of hair follicles in *Pla2g10*$^{+/+}$ but not in *Pla2g10*$^{-/-}$ mice (Fig. 6*B*). Staining of the hair shaft was again nonspecific, as it was also obvious in *Pla2g10*$^{-/-}$ skin (Fig. 6*B*). Analyses of the developmental expression of *Pla2g10* mRNA in mouse skin by quantitative RT-PCR revealed that its expression was low at E17.5 (hair folliculogenesis stage), increased to a maximum expression level by P10 (anagen), declined to the basal level at P15–20 (catagen to telogen), and again began to increase at P25 (re-entry into the next anagen) (Fig. 6*C*). These results suggest that the expression of sPLA$_2$-X is confined to hair follicles, being synchronized with hair cycling exhibiting a pattern of increased expression during the hair-growing anagen phase and decreased expression during the hair-retracting/resting catagen to telogen phases.

To further verify the hair follicular localization of sPLA$_2$-X, hair follicles as well as epidermis were isolated by laser-capture microdissection from the mid-dorsal skin at P8 (Fig. 7*A*), a period of mid-anagen when the expression of sPLA$_2$-X reached a nearly maximal level (Fig. 6*C*). Pools from hair follicles and epidermis obtained thus far were then subjected to quantitative RT-PCR for several marker genes known to localize specifically in each skin compartment. Preferential enrichment of *S100a9*, *Krt1*, and *Krt14* in the epidermis fraction and *Krt71*, *Krt85*, and *Krt33a* in the hair follicle fraction indicated that the microdissection of each skin compartment had been successful (Fig. 7*B*). Importantly, *Pla2g10* mRNA was detected in the hair follicle, but not in the epidermis, fraction (Fig. 7*C*), thus confirming the hair follicular localization of sPLA$_2$-X in mouse skin. We then reasoned that if sPLA$_2$-X indeed exists in hair follicles, its expression would be compromised in the other mouse line with hair abnormality. To this end, we examined the expression of *Pla2g10* mRNA in the skin of phospholipase Cδ1-deficient (*Plcd1*$^{-/-}$) mice, which exhibit postnatal distortion of hair follicles (30). As expected, the expression of *Pla2g10* mRNA was hair cycle-dependent in *Plcd1*$^{+/+}$ skin (in agreement with Fig. 6*C*), whereas it was markedly reduced in *Plcd1*$^{-/-}$ skin at each postnatal point (supplemental Fig. S5).

It was notable in wild-type mice that the two COX isoforms COX-1 (*Ptgs1*) and COX-2 (*Ptgs2*) were distributed predominantly in the epidermis and hair follicles, respectively, and that mPGES-1 (*Ptges*) was detected in the epidermis in marked preference to hair follicles, whereas other PGE synthases (*Ptges2* and *Ptges3*) were evenly distributed in both fractions (Fig. 7*C*). These results suggest that the PGE$_2$-biosynthetic enzymes are spatially segregated in distinct skin compartments and that the epidermal distribution of COX-1 and mPGES-1 could account for their increased expression in *PLA2G10*-Tg mice (Fig. 4*C*), where the epidermis is highly hyperplasic (Fig. 2).

Hair Follicle Abnormality in Pla2g10$^{-/-}$ *Mice*—Given that the expression of *Pla2g10* mRNA in hair follicles reached a maximum level during anagen (Fig. 6*C*), we reassessed the hair histology of *Pla2g10*$^{-/-}$ and *Pla2g10*$^{+/+}$ skins at the mid-anagen stage (P8). In contrast to the normal appearance of hair shafts in *Pla2g10*$^{+/+}$ mice, those in *Pla2g10*$^{-/-}$ mice were frequently bent (Fig. 8*A*), although the number of hair follicles was similar between the genotypes (Fig. 8*B*). Quantitative RT-PCR of the hair follicle fraction, which had been isolated by microdissection (Fig. 7), revealed that the expression of the hair keratin *Krt85*, but not *Krt6a* and *Krt17*, was substantially lower in *Pla2g10*$^{-/-}$ mice than in *Pla2g10*$^{+/+}$ mice (Fig. 8*C*), consistent with the microarray analysis (Fig. 5).

To further verify the ultrastructural abnormalities in hair follicles, we carried out transmission electron microscopy of mouse skin (Fig. 8, *D–F*). The hair follicle consists broadly of five distinctive layers: ORS, IRS, cuticle (*Cu*), hair cortex (*Cx*), and medulla (*M*) from the outermost to innermost layers. Each hair follicle has an ORS, which surrounds the follicle like a sleeve all the way to the bulb and is distinct from other epidermal components of the hair follicle. The cells of the ORS con-

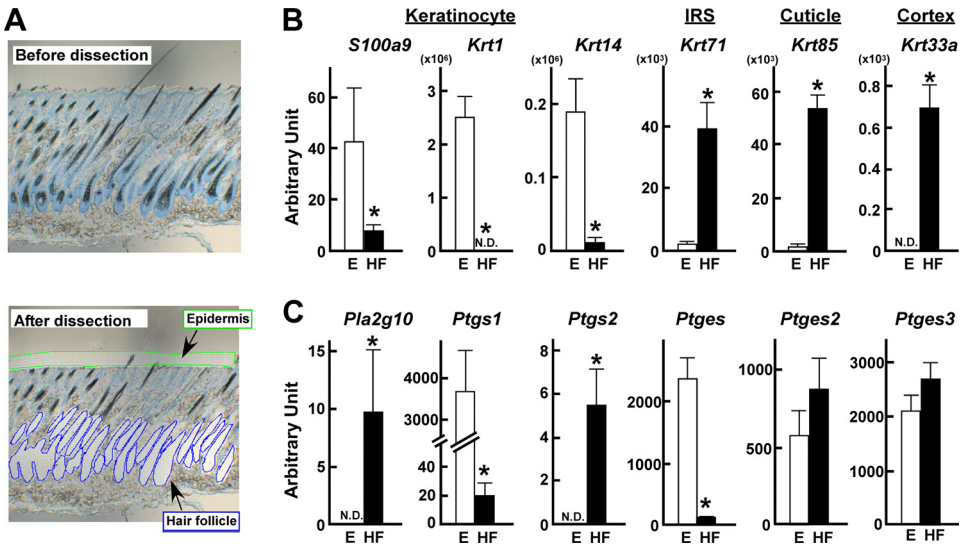

FIGURE 7. **Compartmentalization of endogenous sPLA$_2$-X and PG-biosynthetic enzymes in mouse skin.** *A*, mouse skin sections (P8) before (*upper*) and after (*lower*) microdissection of hair follicles (*HF*) and epidermis (*E*) were stained with toluidine blue. Total RNAs were extracted from the microdissected hair follicle or epidermis fraction followed by quantitative RT-PCR of various genes. *B*, expression levels of marker genes associated with epidermal keratinocytes (*S100a9*, *Krt1*, and *Krt14*) and hair follicular compartments (*Krt71*, *Krt85*, and *Krt33a*) in the epidermis (*E*; *open columns*) and hair follicle (*HF*; *solid columns*) fractions are shown. *C*, expression levels of mRNAs for *Pla2g10* and PG-biosynthetic enzymes in the epidermis and hair follicle fractions are shown. Relative abundance of these transcripts was normalized against the constitutive expression of *Actb* (β-actin) mRNA. Data are the means ± S.E. ($n = 6$; *, $p < 0.05$). *N.D.*, not detected.

tain clearly vacuolated cytoplasm because of the presence of large amounts of glycogen. The cells at the periphery are more vacuolated than those in the axial border, which show a relatively intact cytoplasm. The store of glycogen in the ORS is probably utilized as a local supply of energy and materials for bulbar cell activities. In contrast, the ORS in *Pla2g10*$^{-/-}$ mice was noticeably thinner than that in wild-type mice (Fig. 8*D* and supplemental Fig. S6). Many of the vacuoles in ORS cells of *Pla2g10*$^{-/-}$ mice were disorganized and small relative to those of *Pla2g10*$^{+/+}$ mice (Fig. 8*E*, *a* and *d*). Furthermore, in ORS cells of *Pla2g10*$^{-/-}$ mice, many of the mitochondria were swollen, and the pattern of tonofilaments was irregular (Fig. 8*E*, *d*). Because ORS cells at the mid-anagen stage are undergoing active cell division, the nuclei in ORS cells of *Pla2g10*$^{+/+}$ mice showed a euchromatin structure (Fig. 8*E*, *a*). In contrast, the nuclei in the *Pla2g10*$^{-/-}$ ORS had a heterochromatin configuration, which is indicative of cell growth arrest or retardation (Fig. 8*E*, *d*). The companion layer, which is focally present in the innermost part of the ORS, is more flattened than the other cells of the ORS and does not contain glycogen. However, the border of the companion layer and ORS in the *Pla2g10*$^{-/-}$ follicles was vague compared with that in the *Pla2g10*$^{+/+}$ follicles (Fig. 8, *D* and *E*, *a* and *d*). The IRS of the hair follicle constitutes a layered structure that extends from the base of the bulb to the isthmus, consisting of three distinct layers of epithelial cells known as Henle's layer (*He*), Huxley's layer (*Hx*), and IRS cuticle (*Ci*). The ultrastructure of these IRS layers did not differ between the genotypes (Fig. 8*E*, *b* and *e*). The hair shaft (cuticle, cortex, and medulla) is the cylindrical, keratinized, and often pigmented filament that can be seen in the upper skin, consisting mainly of dead cells that have turned into keratin filaments and binding material together with small amounts of water. Although structural abnormalities of the hair shaft were barely seen in *Pla2g10*$^{-/-}$ mice, melanin granules in the cortex were fewer in *Pla2g10*$^{-/-}$ mice than in *Pla2g10*$^{+/+}$ mice (Fig. 8*E*, *c* and *f*). The bulb is a deep, bulbous portion of the follicle that surrounds the dermal papilla. Although the dermal papilla is responsible for directing and dictating the embryonic generation of a hair follicle, the bulb is the structure of actively growing cells that eventually produce the long fine hair cylinder. There were no morphologic differences in the hair bulb between the genotypes (Fig. 8*F*). Thus, even though endogenous sPLA$_2$-X is dispensable for the central pathway for hair development, its absence in hair follicles results in ORS hypoplasia leading to modest hair shaft abnormality.

Unusual Up-regulation of PGE$_2$ Synthesis in Hair Follicle of Pla2g10$^{-/-}$ *Mice*—Having established that sPLA$_2$-X is a hair follicular sPLA$_2$ that participates in the control of hair follicle homeostasis, we anticipated that the absence of this enzyme would decrease the level of hair follicular prostanoids. Unexpectedly, however, the level of PGE$_2$ in the microdissected hair follicle fraction was unusually increased rather than decreased in *Pla2g10*$^{-/-}$ mice in comparison with *Pla2g10*$^{+/+}$ mice (Fig. 9*A*). To gain insight into this unexpected elevation of PGE$_2$ in *Pla2g10*$^{-/-}$ hair follicles, we examined the expression of enzymes in the PGE$_2$ biosynthetic pathway in the microdissected hair follicle fraction by quantitative RT-PCR. Remarkably, the expression levels of COX-2 (*Ptgs2*) and to a lesser extent mPGES-1 (*Ptges*), but not other PGE synthases (*Ptges2* and *Ptges3*) and the hair follicle PGE receptor EP4 (*Ptger4*), were increased in hair follicles of *Pla2g10*$^{-/-}$ mice relative to those of *Pla2g10*$^{+/+}$ mice (Fig. 9*B*). In contrast, the expression of COX and PGES enzymes (Fig. 9*C*) as well as the level of PGE$_2$ (Fig. 9*A*) in the epidermis fraction was similar between the genotypes. These results suggest that, unlike sPLA$_2$-X overexpressed ectopically at a superphysiological level in *PLA2G10*-Tg mice (Fig. 4), endogenous sPLA$_2$-X restricted to the anagen hair follicles is not linked to local PGE$_2$ synthesis;

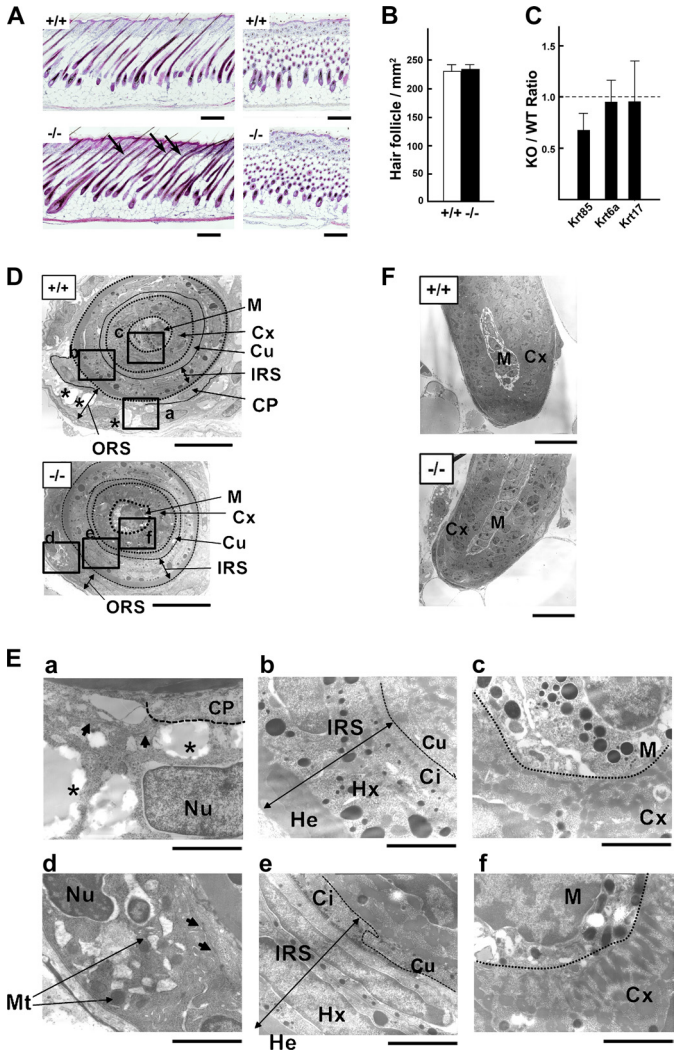

FIGURE 8. ***Pla2g10*$^{-/-}$ mice harbor hair follicle abnormality.** *A*, histology of hair follicles in *Pla2g10*$^{+/+}$ and *Pla2g10*$^{-/-}$ mice at P8 is shown. Abnormal hair follicles are shown by *arrows*. *Bars*, 500 μm. *B*, hair follicular density was similar between *Pla2g10*$^{+/+}$ and *Pla2g10*$^{-/-}$ mice. *C*, reduced hair keratin (*Krt85*) expression in the hair follicle fraction from *Pla2g10*$^{-/-}$ mice relative to *Pla2g10*$^{+/+}$ mice, as assessed by quantitative RT-PCR, is shown. *D–F*, transmission electron microscopies of hair follicles in *Pla2g10*$^{+/+}$ and *Pla2g10*$^{-/-}$ skins are shown. *D*, five distinct layers (ORS, IRS, cuticle (*Cu*), cortex (*Cx*), and medulla (*M*)) as well as the companion layer (*Cp*) (a single layered band of flat and vertically oriented cells between the ORS and IRS) are indicated. As compared with the ORS layer of *Pla2g10*$^{+/+}$ mice, that of *Pla2g10*$^{-/-}$ mice was thin. *Boxed areas in D* are magnified in *E*. *Bars*, 10 μm. *E*, ORS cells in *Pla2g10*$^{+/+}$ mice contained nutrient-rich cytoplasmic vacuoles (*asterisks*) and the nucleus (*Nu*) in a euchromatin configuration (*a*), whereas those cells in *Pla2g10*$^{-/-}$ mice had smaller vacuoles, heterochromatin nucleus, and swollen mitochondria (*Mt*) (*d*). *Arrows* indicate tonofilaments. Although the structures of the IRS and hair shaft appeared similar between *Pla2g10*$^{+/+}$ (*b* and *c*) and *Pla2g10*$^{-/-}$ (*e* and *f*) mice, there were fewer melanin granules in the medulla of the null mice than in that of the wild-type mice. *Bars*, 2 μm. *He*, Henle's layer; *Hx*, Huxley's layer; *Ci*, IRS cuticle. *F*, the ultrastructure of the hair bulb appeared normal in *Pla2g10*$^{-/-}$ mice. *Bars*, 10 μm.

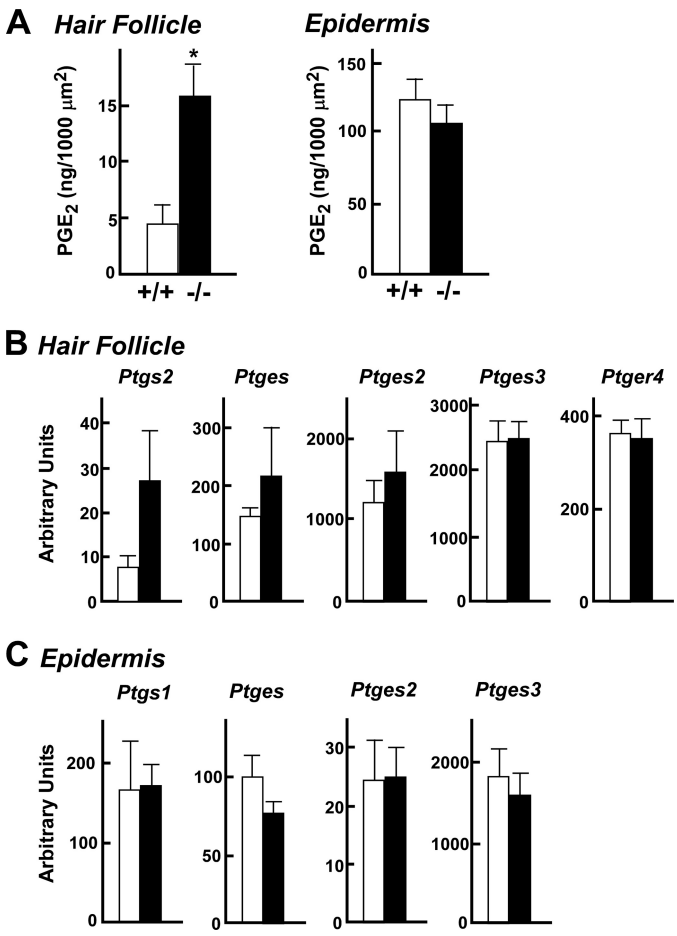

FIGURE 9. **Increased COX-2 expression and PGE$_2$ synthesis in hair follicles of *Pla2g10*$^{-/-}$ mice.** *A*, hair follicle and epidermis fractions were isolated by laser-capture microdissection from the skins of *Pla2g10*$^{+/+}$ (*open columns*) and *Pla2g10*$^{-/-}$ (*solid columns*) mice ($n = 6$). PGE$_2$ contents in the isolated hair follicle or epidermis fractions were quantified by enzyme immunoassay. *B* and *C*, quantitative RT-PCR of various mRNAs for PGE$_2$ synthesis and its receptor in hair follicles (*B*) and epidermis (*C*) is shown. Relative abundance of their transcripts was normalized relative to the constitutive expression of *Actb* mRNA. Data are the means ± S.E. ($n = 6$).

rather, it may negatively regulate the expression of the PGE$_2$ biosynthetic components (COX-2 and mPGES-1) through an unknown mechanism (see "Discussion"). Accordingly, the absence of sPLA$_2$-X in hair follicles causes exaggerated PGE$_2$ signaling, which may in turn perturb hair follicle homeostasis. This event seems to be compatible with hair defects observed in skin-specific COX-2-Tg mice (10, 11).

DISCUSSION

The hair cycle relies on an elegant and coordinated balance of stimulatory and inhibitory signals, which are spatially and temporally regulated in the hair follicle niche through orchestrated actions of various growth or differentiation factors and their inhibitors, transcription factors, and lipids (1–3). Clarification of the molecular mechanisms underlying hair regulation by these factors would provide opportunities for new therapeutic approaches to the treatment of individuals with hair loss, which can cause considerable psychological distress in most of those affected. In this study we have provided evidence that sPLA$_2$-X is expressed in hair follicles in synchrony with the postnatal hair cycle and participates in hair quality control. To our knowledge, this is the first demonstration that this particular sPLA$_2$ isoform plays a homeostatic role in a highly specialized skin compartment, *i.e.* the hair follicle, in addition to its reported roles in diverse pathophysiological events including asthma, ischemic myocardial injury, aneurysm, adiposity, adrenal steroid secretion, and fertility (17, 18, 23–28).

PLA2G10-Tg Mice Display Alopecia as Well as Epidermal Hyperplasia—Probably, the most striking evidence for the potential role of sPLA$_2$ in the skin has been gained from studies employing *PLAG2A*-Tg mice, which exhibit almost total alopecia with no signs of inflammation (19), although the C57BL/6 mouse strain intrinsically lacks sPLA$_2$-IIA as a result of a frameshift mutation of its gene (20). Although several previous studies have reported expression and localization of various sPLA$_2$s in skin or cultured keratinocytes (52–55), variations in detection methodology and incomplete functional assessments have cast doubt on the specific roles of sPLA$_2$s in complex skin niches.

In this study we found that Tg overexpression of sPLA$_2$-X leads to alopecia (Figs. 1 and 2). This observation seems important as, unlike sPLA$_2$-IIA that is absent from mouse skin, sPLA$_2$-X is expressed endogenously in mouse hair follicles (Figs. 6 and 7). However, although *PLA2G2A*-Tg mice are permanently alopecic (19), the hairless phenotype of *PLA2G10*-Tg mice is evident only over a period corresponding to the catagen to telogen phase of the postnatal hair cycle. In contrast to the group II subfamily of sPLA$_2$s, which are catalytically active once synthesized, sPLA$_2$-X has an N-terminal propeptide that has to be removed before its activation (22, 49). Interestingly, the PLA$_2$ enzymatic activity in skin homogenates of *PLA2G10*-Tg mice is transiently elevated before the hair loss, in accordance with the appearance of the mature form of sPLA$_2$-X protein (Fig. 1), suggesting that proteolytic activation of sPLA$_2$-X occurs in mouse skin during the early hair cycle. This temporary activation of sPLA$_2$-X, as opposed to constitutive expression of active sPLA$_2$-IIA, may account for the transient *versus* permanent appearance of skin abnormalities in *PLA2G10*- and *PLA2G2A*-Tg mice, respectively. In contrast to the remarkable skin phenotype, many other tissues in *PLA2G10*-Tg mice displayed no apparent histological abnormalities (supplemental Fig. S1), probably because the overexpressed sPLA$_2$-X remains as an inactive zymogen unless inflammation occurs (29). Thus, mouse skin may have some particular protease machinery that leads to proteolytic processing of sPLA$_2$-X under physiological conditions. In fact, unique and highly regulated protease/protease inhibitor networks are present in the skin, and disturbance of their balance could lead to faulty processing of hair follicle development and epidermal differentiation (40–48). Although the skin proteases responsible for sPLA$_2$-X activation remain to be identified, kallikreins may be a candidate, as Tg overexpression of kallikreins leads to a similar skin phenotype (41), expression of kallikreins is markedly increased in *PLA2G10*-Tg skin (supplemental Fig. S3), and the propeptide sequence of sPLA$_2$-X can be cleaved by kallikrein family proteases.

Our previous studies of Tg overexpression of sPLA$_2$ isoforms in mice in combination with a lipidomics approach have led to the identification of potential *in vivo* actions of sPLA$_2$-V on lung surfactant PC (29) and sPLA$_2$-III on lipoprotein PC (32). However, although sPLA$_2$-X is the most potent sPLA$_2$ isoform with the ability to hydrolyze PC in intact mammalian cell membranes (56, 57), levels of PC as well as phosphatidylinositol and phosphatidylserine were unchanged in the skin of *PLA2G10*-Tg mice. Strikingly, hydrolysis of particular PE species giving rise to free AA, eicosapentaenoic acid, and docosahexaenoic acid, as well as C18:0 and C18:1 lysophosphatidylethanolamine, occurred in *PLA2G10*-Tg mice (Figs. 3 and 4), suggesting that sPLA$_2$-X can preferentially hydrolyze PUFA-containing PE species in mouse skin. Given that sPLA$_2$-X can hydrolyze both PC and PE equally *in vitro* (21, 56) and that PE usually resides in the inner leaflet of the plasma membrane, our results suggest that a pool of PUFA-containing PE species possibly secreted into the skin microenvironment or enriched in a particular membrane microdomain may become available for sPLA$_2$-X-directed hydrolysis. Because PE is also a good substrate for sPLA$_2$-IIA (6, 7), the shared skin phenotype between *PLA2G2A*-Tg and *PLA2G10*-Tg mice might primarily result from increased PE hydrolysis. Importantly, because no biochemical analysis of the alopecic phenotype of *PLA2G2A*-Tg mice has been conducted (19), the present study has provided the first biochemical insights into sPLA$_2$-triggered phospholipid metabolism in the context of skin biology.

The AA produced by overexpressed sPLA$_2$-X can be further converted to biologically active metabolites in the skin. Indeed, we found a notable increase of PGE$_2$, a major COX metabolite produced by keratinocytes (55), in *PLA2G10*-Tg mice (Fig. 4). It has been reported that Tg overexpression of COX-2 in mouse skin results in increased PGE$_2$ generation accompanied by hair loss as well as by abnormal epidermal differentiation leading to hyperplasia and dysplasia with little sign of inflammation (9), events that are strikingly similar to those observed in *PLA2G10*-Tg mice. PGE$_2$ directly promotes keratinocyte proliferation in culture via EP2, a G protein-coupled PGE receptor, and Tg overexpression of EP2 also results in epidermal abnormality (59). Another PGE receptor, EP4, is expressed in the ORS of anagen hair follicles (8, 9), and elevated expression of EP4 as well as COX-2 is associated with human scarring alopecia (12). On the basis of these observations, it is likely that the overwhelming majority of PGE$_2$ signaling may be linked, at least partly, with the hair follicle and epidermal abnormalities observed in *PLA2G10*-Tg mice. Additionally, coordinated increases in the expression of epidermal-type LOX enzymes, whose mutations or deletions cause epidermal abnormalities such as ichthyosis (50, 51), may be associated with epidermal hyperplasia in *PLA2G10*-Tg mice.

Pla2g10-deficient Mice Reveal the Intrinsic Role of sPLA$_2$-X in Hair Follicle Homeostasis—The marked skin abnormalities manifested in *PLA2G10*-Tg mice prompted us to examine whether endogenous sPLA$_2$-X would act as an intrinsic regulator of skin homeostasis. Our present studies employing immunohistochemistry as well as real-time RT-PCR analyses combined with a microdissection technique have provided evidence that it is in the hair follicle and not in the epidermis, as has been reported previously (52, 54), where sPLA$_2$-X is intrinsically expressed. This is supported by the following observations. (i) immunohistochemical staining of sPLA$_2$-X in mouse skin is distributed solely in the outermost layers of hair follicles, whereas it is absent in *Pla2g10*$^{-/-}$ mice (Fig. 6, *A* and *B*). (ii) Expression of *Pla2g10* mRNA in mouse skin shows a pattern synchronized with hair cycling (Fig. 6*C*). (iii) In the skin of *Plcd1*$^{-/-}$ mice, which have distorted hair follicles (30), *Pla2g10* mRNA expression is markedly reduced (supplemental Fig. S5).

(iv) After laser-capture microdissection, *Pla2g10* mRNA is enriched in the hair follicle fraction but not in the epidermis fraction (Fig. 7). (v) *Pla2g10*$^{-/-}$ mice display notable, albeit mild, abnormalities in hair follicles but not in the epidermis (Figs. 5, 8, and 9). Our finding that sPLA$_2$-X is expressed in a restricted compartment within the skin niche (*i.e.* the ORS of hair follicles) in correlation with hair cycling, showing high expression during anagen and low expression during catagen-telogen, highlights an unexplored physiological role of this particular sPLA$_2$ subtype in hair follicle homeostasis.

Interestingly, similar hair cycle-related expression profiles in the ORS or IRS of hair follicles have also been observed for several other hair-regulating factors that participate in the regulation of anagen-catagen or telogen-anagen transition and thereby in proper hair growth (60–67). Indeed, even though the hair phenotype of *Pla2g10*$^{-/-}$ mice appeared mild, our results revealed substantial reductions in a panel of genes encoding hair keratins and keratin-associated proteins as well as genes encoding the hair shaft-regulatory transcription factors (Fig. 5), suggesting delayed hair growth. In contrast, genes for the epidermis were unaffected by the lack of sPLA$_2$-X, in agreement with the intrinsic distribution of this enzyme in the follicular ORS but not in the interfollicular epidermis. Moreover, in mid-anagen, the ORS above the hair bulb of *Pla2g10*$^{-/-}$ mice was thin, contained swollen mitochondria and fewer nutrient-rich vacuolar components, and showed evident growth retardation, perhaps causing focal twisting of subdermal hairs (Fig. 8). This is in contrast with the ORS of *PLA2G10*-Tg mice, which was strikingly hyperplasic (Fig. 2). Thus, sPLA$_2$-X may contribute to the homeostasis of hair follicular ORS by promoting the proper growth of ORS keratinocytes. Perturbed growth and survival of ORS cells ultimately lead to the deficit in hairs (68).

Our present analysis employing laser-capture microdissection has demonstrated distinct compartmentalization of COX-1 and COX-2 in the epidermis and hair follicles, respectively, in mouse skin under physiological conditions (Fig. 7*C*). This finding is consistent with a previous study showing that COX-1 is localized predominantly in the interfollicular spinous and granular layers of the epidermis but not in follicular epithelial cells of cycling hair follicles, whereas COX-2 expression is hair cycling-dependent, becoming apparent in elongated hair germs and hair pegs in the course of pelage hair follicle morphogenesis, later on in the ORS of the distal and proximal hair follicles, declining in catagen and telogen, and then being re-induced in the ORS of anagen hair follicles (9). Because the expression of sPLA$_2$-X in the ORS is also hair cycling-dependent (Fig. 6*C*), we had anticipated that sPLA$_2$-X and COX-2 at the same location would be functionally coupled to provide a hair follicular pool of PGE$_2$. Surprisingly, however, the level of hair follicular PGE$_2$ was elevated rather than reduced by the absence of sPLA$_2$-X. Consistent with this unexpected finding, the hair follicular expression of COX-2 and to a lesser extent mPGES-1 was substantially higher in *Pla2g10*$^{-/-}$ mice than in *Pla2g10*$^{+/+}$ mice (Fig. 9). These results led us to conclude that endogenous sPLA$_2$-X is not coupled with PGE$_2$ synthesis in hair follicles; rather, its deficiency results in aberrant COX-2 expression leading to increased PGE$_2$ synthesis, thereby mimicking the situation in skin-specific COX-2 Tg mice, which display hair abnormality (9, 58). Therefore, the mechanisms underlying hair abnormalities resulting from overexpression *versus* deletion of sPLA$_2$-X appear to be distinct.

Although the molecular mechanism whereby deficiency of sPLA$_2$-X leads to dysregulated COX-2 expression in hair follicles is still unclear, it is tempting to speculate that some lipid product(s) produced by sPLA$_2$-X in this particular skin compartment may facilitate local induction of COX-2 and thereby overproduction of PGE$_2$. LPA may be such a candidate, as mutations in the human *P2Y5* gene (encoding LPA$_6$ receptor) cause autosomal recessive wooly hair with hypotrichosis, although this speculation argues against the fact that the absence of LPA$_6$ signaling perturbs the IRS rather than the ORS (7). It has been recently reported that sPLA$_2$-X negatively regulates liver X receptor (LXR) or peroxisome proliferator-activating receptor (PPAR) signaling through production of PUFA in macrophages, adrenal cells, and adipocytes (26, 27, 69). Considering that the liver X receptor/peroxisome proliferator-activating receptor signaling pathway can diversely affect COX-2/mPGES-1-dependent PGE$_2$ production (70–72) and that dysregulation of hair follicular PPARγ is linked to alopecia (12), sPLA$_2$-X-dependent lipid product(s) might modulate PGE$_2$ signaling through the lipid-sensing nuclear receptors in hair follicles. Alternatively, because sPLA$_2$-X can potently hydrolyze lipoproteins (32) and because lipoprotein abnormality can cause hair loss (74), deficiency of sPLA$_2$-X might locally perturb lipoprotein-mediated lipid transport within a hair follicle niche, thereby causing atrophy of nutrient-rich vacuoles in the ORS. Nevertheless, future identification of the sPLA$_2$-X-regulated lipid pathway linked to ORS homeostasis would increase our understanding of the importance of lipids in skin biology. As an associated finding, we observed a notable decrease of melanin granules in hairs of *Pla2g10*$^{-/-}$ mice (Fig. 8). This may reflect the observation that sPLA$_2$-X facilitates melanin synthesis and pigmentation through production of lysophosphatidylcholine *in vitro* (75). Alternatively, in view of the hypothetical sPLA$_2$-X/lipid-sensing nuclear receptor connection mentioned above, regulation of melanin synthesis by PPARγ (76, 77) might underlie the decreased pigmentation of *Pla2g10*$^{-/-}$ hairs.

Future Prospects—Given that sPLA$_2$-X essentially works as a hair modulator in anagen hair follicles, what is the significance of the abnormalities in the epidermis and sebaceous glands in *PLA2G10*-Tg mice? Lipids produced by epidermal keratinocytes and sebaceous glands play additional important roles in skin homeostasis (13, 14). Terminally differentiated epidermal keratinocytes secrete neutral lipids and fatty acids into the intercellular spaces of cornified envelopes, where they form a skin permeability barrier that prevents water loss from the body and also provides protection from invading pathogens and environmental toxins. Particularly, free fatty acids in the skin are important for acidification, integrity, and barrier function of the stratum corneum, and hydrolysis of phospholipids by certain sPLA$_2$(s) has been proposed to be crucial for the supply of fatty acids into the interspace of corneocytes (78–80). Sebaceous glands produce and secrete lipid-rich sebum into the hair canal that empties out to the skin surface. In fact, expression of several lipogenic genes such as *Elovl3* and *Scd1*, mutations of

which result in cutaneous phenotypes (13, 14), was also elevated in *PLA2G10*-Tg skin (data not shown), suggesting a connection between sPLA$_2$-directed perturbation of the lipid milieu and epidermal or sebaceous gland disorders. However, neither sPLA$_2$-X (this study) nor sPLA$_2$-IIA (9) is endogenously expressed in the epidermis or sebaceous glands of C57BL/6 mice, raising a question about the physiological relevance of the epidermal and sebaceous gland hyperplasia induced by Tg overexpression of a particular sPLA$_2$ isoform.

The following possibilities are considered. First, considering that the hair follicle, epidermis, and sebaceous gland are contiguous, primary action of the overexpressed sPLA$_2$-X on hair follicles might eventually alter the differentiation fate of skin stem cells at the bulge into upward (epidermal and sebaceous gland keratinocytes) rather than downward (follicular keratinocytes) directions, thereby altering the gene balance toward terminal epidermal differentiation over hair development. Indeed, hair abnormalities caused by deletion or mutations of various genes are often accompanied by epidermal and sebaceous gland abnormalities as well (73, 81, 82). Second, even though sPLA$_2$-X is undetectable in the epidermis under sterile conditions, it might be induced in the epidermis under certain pathologic conditions such as dermatitis, infection, and cancer, where it might play some unidentified roles through modulation of epidermal phospholipid metabolism. Third, although the results of sPLA$_2$-X overexpression on skin are not reciprocated by those of sPLA$_2$-X deficiency (*i.e.* the defects in the knock-out mice are very modest compared with the effects in the Tg mice), the weak phenotype of sPLA$_2$-X deficiency might be due to compensation by other sPLA$_2$(s) expressed in mouse skin (52, 54). Indeed, the epidermal phenotype of *PLA2G10*-Tg mice might mirror the function of other sPLA$_2$(s) that is intrinsically expressed in the epidermis, as we have recently found that a particular sPLA$_2$ subtype (distinct from sPLA$_2$-X) is highly expressed in mouse epidermis and that manipulation of its gene in mice causes striking epidermal abnormalities with dysregulated lipid signaling and epidermal barrier function, which are now under investigation.[4]

Finally, in view of previous reports showing that several sPLA$_2$s including sPLA$_2$-X are expressed in human epidermal keratinocytes (52, 53), sPLA$_2$-X might participate in the homeostatic control of lipid machinery in the epidermis of humans. Nevertheless, the spatiotemporal expression profile of a full set of sPLA$_2$s in healthy or diseased human skin would need careful reevaluation in the context of hair cycling, epidermal proliferation and differentiation, dermal inflammation, and wound healing. As a matter of fact, the spatiotemporal localization of sPLA$_2$s in human hair follicles is entirely unknown. Given that millions of people suffer from hair loss that can be caused by various factors including genetic mutations, hormonal imbalances, immunological abnormalities, environmental exposures, or psychological stresses, full elucidation of the lipid networks regulated by sPLA$_2$s in humans would be helpful for a novel strategy for treatment of alopecia.

[4] K. Yamamoto and M. Murakami, unpublished observation.

Acknowledgments—We thank Dr. Michael Gelb (University of Washington, Seattle, WA) and Dr. Shinji Hatakeyama (Novartis Pharma, Tsukuba, Japan) for providing rabbit polyclonal and mouse monoclonal anti-human sPLA$_2$-X antibodies, respectively.

REFERENCES

1. Alonso, L., and Fuchs, E. (2006) *J. Cell Sci.* **119,** 391–393
2. Fuchs, E. (2007) *Nature* **445,** 834–842
3. Blanpain, C., and Fuchs, E. (2009) *Nat. Rev. Mol. Cell Biol.* **10,** 207–217
4. Kupper, T. S., and Fuhlbrigge, R. C. (2004) *Nat. Rev. Immunol.* **4,** 211–222
5. Lowes, M. A., Bowcock, A. M., and Krueger, J. G. (2007) *Nature* **445,** 866–873
6. Colombe, L., Vindrios, A., Michelet, J. F., and Bernard, B. A. (2007) *Exp. Dermatol.* **16,** 762–769
7. Pasternack, S. M., von Kügelgen, I., Aboud, K. A., Lee, Y. A., Rüschendorf, F., Voss, K., Hillmer, A. M., Molderings, G. J., Franz, T., Ramirez, A., Nürnberg, P., Nöthen, M. M., and Betz, R. C. (2008) *Nat. Genet.* **40,** 329–334
8. Torii, E., Segi, E., Sugimoto, Y., Takahashi, K., Kabashima, K., Ikai, K., and Ichikawa, A. (2002) *Biochem. Biophys. Res. Commun.* **290,** 696–700
9. Müller-Decker, K., Leder, C., Neumann, M., Neufang, G., Bayerl, C., Schweizer, J., Marks, F., and Fürstenberger, G. (2003) *J. Invest. Dermatol.* **121,** 661–668
10. Neufang, G., Furstenberger, G., Heidt, M., Marks, F., and Müller-Decker, K. (2001) *Proc. Natl. Acad. Sci. U.S.A.* **98,** 7629–7634
11. Bol, D. K., Rowley, R. B., Ho, C. P., Pilz, B., Dell, J., Swerdel, M., Kiguchi, K., Muga, S., Klein, R., and Fischer, S. M. (2002) *Cancer Res.* **62,** 2516–2521
12. Karnik, P., Tekeste, Z., McCormick, T. S., Gilliam, A. C., Price, V. H., Cooper, K. D., and Mirmirani, P. (2009) *J. Invest. Dermatol.* **129,** 1243–1257
13. Westerberg, R., Tvrdik, P., Undén, A. B., Månsson, J. E., Norlén, L., Jakobsson, A., Holleran, W. H., Elias, P. M., Asadi, A., Flodby, P., Toftgård, R., Capecchi, M. R., and Jacobsson, A. (2004) *J. Biol. Chem.* **279,** 5621–5629
14. Zheng, Y., Eilertsen, K. J., Ge, L., Zhang, L., Sundberg, J. P., Prouty, S. M., Stenn, K. S., and Parimoo, S. (1999) *Nat. Genet.* **23,** 268–270
15. Cordeddu, V., Di Schiavi, E., Pennacchio, L. A., Ma'ayan, A., Sarkozy, A., Fodale, V., Cecchetti, S., Cardinale, A., Martin, J., Schackwitz, W., Lipzen, A., Zampino, G., Mazzanti, L., Digilio, M. C., Martinelli, S., Flex, E., Lepri, F., Bartholdi, D., Kutsche, K., Ferrero, G. B., Anichini, C., Selicorni, A., Rossi, C., Tenconi, R., Zenker, M., Merlo, D., Dallapiccola, B., Iyengar, R., Bazzicalupo, P., Gelb, B. D., and Tartaglia, M. (2009) *Nat. Genet.* **41,** 1022–1026
16. Klar, J., Schweiger, M., Zimmerman, R., Zechner, R., Li, H., Törmä, H., Vahlquist, A., Bouadjar, B., Dahl, N., and Fischer, J. (2009) *Am. J. Hum. Genet.* **85,** 248–253
17. Lambeau, G., and Gelb, M. H. (2008) *Annu. Rev. Biochem.* **77,** 495–520
18. Murakami, M., Taketomi, Y., Girard, C., Yamamoto, K., and Lambeau, G. (2010) *Biochimie* **92,** 561–582
19. Grass, D. S., Felkner, R. H., Chiang, M. Y., Wallace, R. E., Nevalainen, T. J., Bennett, C. F., and Swanson, M. E. (1996) *J. Clin. Invest.* **97,** 2233–2241
20. MacPhee, M., Chepenik, K. P., Liddell, R. A., Nelson, K. K., Siracusa, L. D., and Buchberg, A. M. (1995) *Cell* **81,** 957–966
21. Murakami, M., Kambe, T., Shimbara, S., Higashino, K., Hanasaki, K., Arita, H., Horiguchi, M., Arita, M., Arai, H., Inoue, K., and Kudo, I. (1999) *J. Biol. Chem.* **274,** 31435–31444
22. Masuda, S., Murakami, M., Takanezawa, Y., Aoki, J., Arai, H., Ishikawa, Y., Ishii, T., Arioka, M., and Kudo, I. (2005) *J. Biol. Chem.* **280,** 23203–23214
23. Henderson, W. R., Jr., Chi, E. Y., Bollinger, J. G., Tien, Y. T., Ye, X., Castelli, L., Rubtsov, Y. P., Singer, A. G., Chiang, G. K., Nevalainen, T., Rudensky, A. Y., and Gelb, M. H. (2007) *J. Exp. Med.* **204,** 865–877
24. Fujioka, D., Saito, Y., Kobayashi, T., Yano, T., Tezuka, H., Ishimoto, Y., Suzuki, N., Yokota, Y., Nakamura, T., Obata, J. E., Kanazawa, M., Kawabata, K., Hanasaki, K., and Kugiyama, K. (2008) *Circulation* **117,** 2977–2985
25. Escoffier, J., Jemel, I., Tanemoto, A., Taketomi, Y., Payre, C., Coatrieux, C., Sato, H., Yamamoto, K., Masuda, S., Pernet-Gallay, K., Pierre, V., Hara, S., Murakami, M., De Waard, M., Lambeau, G., and Arnoult, C. (2010) *J. Clin. Invest.* **120,** 1415–1428
26. Shridas, P., Bailey, W. M., Boyanovsky, B. B., Oslund, R. C., Gelb, M. H., and Webb, N. R. (2010) *J. Biol. Chem.* **285,** 20031–20039

27. Li, X., Shridas, P., Forrest, K., Bailey, W., and Webb, N. R. (2010) *FASEB J.* **24,** 4313–4324
28. Zack, M., Boyanovsky, B. B., Shridas, P., Bailey, W., Forrest, K., Howatt, D. A., Gelb, M. H., de Beer, F. C., Daugherty, A., and Webb, N. R. (2011) *Atherosclerosis* **214,** 58–64
29. Ohtsuki, M., Taketomi, Y., Arata, S., Masuda, S., Ishikawa, Y., Ishii, T., Takanezawa, Y., Aoki, J., Arai, H., Yamamoto, K., Kudo, I., and Murakami, M. (2006) *J. Biol. Chem.* **281,** 36420–36433
30. Nakamura, Y., Ichinohe, M., Hirata, M., Matsuura, H., Fujiwara, T., Igarashi, T., Nakahara, M., Yamaguchi, H., Yasugi, S., Takenawa, T., and Fukami, K. (2008) *FASEB J.* **22,** 841–849
31. Murakami, M., Koduri, R. S., Enomoto, A., Shimbara, S., Seki, M., Yoshihara, K., Singer, A., Valentin, E., Ghomashchi, F., Lambeau, G., Gelb, M. H., and Kudo, I. (2001) *J. Biol. Chem.* **276,** 10083–10096
32. Sato, H., Kato, R., Isogai, Y., Saka, G., Ohtsuki, M., Taketomi, Y., Yamamoto, K., Tsutsumi, K., Yamada, J., Masuda, S., Ishikawa, Y., Ishii, T., Kobayashi, T., Ikeda, K., Taguchi, R., Hatakeyama, S., Hara, S., Kudo, I., Itabe, H., and Murakami, M. (2008) *J. Biol. Chem.* **283,** 33483–33497
33. Murakami, M., Masuda, S., Shimbara, S., Ishikawa, Y., Ishii, T., and Kudo, I. (2005) *J. Biol. Chem.* **280,** 24987–24998
34. Bligh, E. G., and Dyer, W. J. (1959) *Can. J. Biochem. Physiol.* **37,** 911–917
35. Houjou, T., Yamatani, K., Nakanishi, H., Imagawa, M., Shimizu, T., and Taguchi, R. (2004) *Rapid Commun. Mass. Spectrom.* **18,** 3123–3130
36. Taguchi, R., Houjou, T., Nakanishi, H., Yamazaki, T., Ishida, M., Imagawa, M., and Shimizu, T. (2005) *J. Chromatogr. B. Analyt. Technol. Biomed. Life Sci.* **823,** 26–36
37. Sato, H., Taketomi, Y., Isogai, Y., Miki, Y., Yamamoto, K., Masuda, S., Hosono, T., Arata, S., Ishikawa, Y., Ishii, T., Kobayashi, T., Nakanishi, H., Ikeda, K., Taguchi, R., Hara, S., Kudo, I., and Murakami, M. (2010) *J. Clin. Invest.* **120,** 1400–1414
38. Ikeda, K., and Taguchi, R. (2010) *Rapid Commun. Mass Spectrom.* **24,** 2957–2965
39. Candi, E., Schmidt, R., and Melino, G. (2005) *Nat. Rev. Mol. Cell Biol.* **6,** 328–340
40. Klucky, B., Mueller, R., Vogt, I., Teurich, S., Hartenstein, B., Breuhahn, K., Flechtenmacher, C., Angel, P., and Hess, J. (2007) *Cancer Res.* **67,** 8198–8206
41. Hansson, L., Bäckman, A., Ny, A., Edlund, M., Ekholm, E., Ekstrand, Hammarström, B., Törnell, J., Wallbrandt, P., Wennbo, H., and Egelrud, T. (2002) *J. Invest. Dermatol.* **118,** 444–449
42. Kishibe, M., Bando, Y., Terayama, R., Namikawa, K., Takahashi, H., Hashimoto, Y., Ishida-Yamamoto, A., Jiang, Y. P., Mitrovic, B., Perez, D., Iizuka, H., and Yoshida, S. (2007) *J. Biol. Chem.* **282,** 5834–5841
43. Leyvraz, C., Charles, R. P., Rubera, I., Guitard, M., Rotman, S., Breiden, B., Sandhoff, K., and Hummler, E. (2005) *J. Cell Biol.* **170,** 487–496
44. Benavides, F., Starost, M. F., Flores, M., Gimenez-Conti, I. B., Guénet, J. L., and Conti, C. J. (2002) *Am. J. Pathol.* **161,** 693–703
45. List, K., Szabo, R., Wertz, P. W., Segre, J., Haudenschild, C. C., Kim, S. Y., and Bugge, T. H. (2003) *J. Cell Biol.* **163,** 901–910
46. Zeeuwen, P. L., van Vlijmen-Willems, I. M., Olthuis, D., Johansen, H. T., Hitomi, K., Hara-Nishimura, I., Powers, J. C., James, K. E., op den Camp, H. J., Lemmens, R., and Schalkwijk, J. (2004) *Hum. Mol. Genet.* **13,** 1069–1079
47. Descargues, P., Deraison, C., Bonnart, C., Kreft, M., Kishibe, M., Ishida-Yamamoto, A., Elias, P., Barrandon, Y., Zambruno, G., Sonnenberg, A., and Hovnanian, A. (2005) *Nat. Genet.* **37,** 56–65
48. Zeeuwen, P. L. (2004) *Eur. J. Cell Biol.* **83,** 761–773
49. Cupillard, L., Koumanov, K., Mattéi, M. G., Lazdunski, M., and Lambeau, G. (1997) *J. Biol. Chem.* **272,** 15745–15752
50. Yu, Z., Schneider, C., Boeglin, W. E., and Brash, A. R. (2005) *Biochim. Biophys. Acta* **1686,** 238–247
51. Eckl, K. M., Krieg, P., Küster, W., Traupe, H., André, F., Wittstruck, N., Fürstenberger, G., and Hennies, H. C. (2005) *Hum. Mutat.* **26,** 351–361
52. Haas, U., Podda, M., Behne, M., Gurrieri, S., Alonso, A., Fürstenberger, G., Pfeilschifter, J., Lambeau, G., Gelb, M. H., and Kaszkin, M. (2005) *J. Invest. Dermatol.* **124,** 204–211
53. Schadow, A., Scholz-Pedretti, K., Lambeau, G., Gelb, M. H., Fürstenberger, G., Pfeilschifter, J., and Kaszkin, M. (2001) *J. Invest. Dermatol.* **116,** 31–39
54. Gurrieri, S., Fürstenberger, G., Schadow, A., Haas, U., Singer, A. G., Ghomashchi, F., Pfeilschifter, J., Lambeau, G., Gelb, M. H., and Kaszkin, M. (2003) *J. Invest. Dermatol.* **121,** 156–164
55. Rys-Sikora, K. E., Pentland, A. P., and Konger, R. L. (2003) *J. Invest. Dermatol.* **120,** 86–95
56. Hanasaki, K., Ono, T., Saiga, A., Morioka, Y., Ikeda, M., Kawamoto, K., Higashino, K., Nakano, K., Yamada, K., Ishizaki, J., and Arita, H. (1999) *J. Biol. Chem.* **274,** 34203–34211
57. Bezzine, S., Koduri, R. S., Valentin, E., Murakami, M., Kudo, I., Ghomashchi, F., Sadilek, M., Lambeau, G., and Gelb, M. H. (2000) *J. Biol. Chem.* **275,** 3179–3191
58. Muller-Decker, K., Neufang, G., Berger, I., Neumann, M., Marks, F., and Furstenberger, G. (2002) *Proc. Natl. Acad. Sci. U.S.A.* **99,** 12483–12488
59. Sung, Y. M., He, G., Hwang, D. H., and Fischer, S. M. (2006) *Oncogene* **25,** 5507–5516
60. Hébert, J. M., Rosenquist, T., Götz, J., and Martin, G. R. (1994) *Cell* **78,** 1017–1025
61. Hansen, L. A., Alexander, N., Hogan, M. E., Sundberg, J. P., Dlugosz, A., Threadgill, D. W., Magnuson, T., and Yuspa, S. H. (1997) *Am. J. Pathol.* **150,** 1959–1975
62. Botchkarev, V. A., Welker, P., Albers, K. M., Botchkareva, N. V., Metz, M., Lewin, G. R., Bulfone-Paus, S., Peters, E. M., Lindner, G., and Paus, R. (1998) *Am. J. Pathol.* **153,** 785–799
63. Foitzik, K., Lindner, G., Mueller-Roever, S., Maurer, M., Botchkareva, N., Botchkarev, V., Handjiski, B., Metz, M., Hibino, T., Soma, T., Dotto, G. P., and Paus, R. (2000) *FASEB J.* **14,** 752–760
64. Cho, Y. M., Woodard, G. L., Dunbar, M., Gocken, T., Jimènez, J. A., and Foley, J. (2003) *J. Invest. Dermatol.* **120,** 715–727
65. Yuhki, M., Yamada, M., Kawano, M., Iwasato, T., Itohara, S., Yoshida, H., Ogawa, M., and Mishina, Y. (2004) *Development* **131,** 1825–1833
66. Vauclair, S., Nicolas, M., Barrandon, Y., and Radtke, F. (2005) *Dev. Biol.* **284,** 184–193
67. Tong, X., and Coulombe, P. A. (2006) *Genes Dev.* **20,** 1353–1364
68. Pena, J. C., Kelekar, A., Fuchs, E. V., and Thompson, C. B. (1999) *EMBO J.* **18,** 3596–3603
69. Shridas, P., Bailey, W. M., Gizard, F., Oslund, R. C., Gelb, M. H., Bruemmer, D., and Webb, N. R. (2010) *Arterioscler Thromb. Vasc. Biol.* **30,** 2014–2021
70. Xu, L., Han, C., Lim, K., and Wu, T. (2006) *Cancer Res.* **66,** 11859–11868
71. Ninomiya, Y., Yasuda, T., Kawamoto, M., Yuge, O., and Okazaki, Y. (2007) *J. Steroid Biochem. Mol. Biol.* **103,** 44–50
72. Li, N., Rivéra-Bermúdez, M. A., Zhang, M., Tejada, J., Glasson, S. S., Collins-Racie, L. A., Lavallie, E. R., Wang, Y., Chang, K. C., Nagpal, S., Morris, E. A., Flannery, C. R., and Yang, Z. (2010) *Proc. Natl. Acad. Sci. U.S.A.* **107,** 3734–3739
73. Glotzer, D. J., Zelzer, E., and Olsen, B. R. (2008) *Dev. Biol.* **315,** 459–473
74. Jong, M. C., Gijbels, M. J., Dahlmans, V. E., Gorp, P. J., Koopman, S. J., Ponec, M., Hofker, M. H., and Havekes, L. M. (1998) *J. Clin. Invest.* **101,** 145–152
75. Scott, G. A., Jacobs, S. E., and Pentland, A. P. (2006) *J. Invest. Dermatol.* **126,** 855–861
76. Kang, H. Y., Chung, E., Lee, M., Cho, Y., and Kang, W. H. (2004) *Br. J. Dermatol.* **150,** 462–468
77. Lee, J. S., Choi, Y. M., and Kang, H. Y. (2007) *Exp. Dermatol.* **16,** 118–123
78. Mao-Qiang, M., Jain, M., Feingold, K. R., and Elias, P. M. (1996) *J. Invest. Dermatol.* **106,** 57–63
79. Fluhr, J. W., Kao, J., Jain, M., Ahn, S. K., Feingold, K. R., and Elias, P. M. (2001) *J. Invest. Dermatol.* **117,** 44–51
80. Fluhr, J. W., Behne, M. J., Brown, B. E., Moskowitz, D. G., Selden, C., Mao-Qiang, M., Mauro, T. M., Elias, P. M., and Feingold, K. R. (2004) *J. Invest. Dermatol.* **122,** 320–329
81. Huelsken, J., Vogel, R., Erdmann, B., Cotsarelis, G., and Birchmeier, W. (2001) *Cell* **105,** 533–545
82. Nakamura, Y., Fukami, K., Yu, H., Takenaka, K., Kataoka, Y., Shirakata, Y., Nishikawa, S., Hashimoto, K., Yoshida, N., and Takenawa, T. (2003) *EMBO J.* **22,** 2981–2991